The Fiordland Current, southwest New Zealand: Mean, interannual variability, and longer-term trends

Mitchell Chandler

Supervised by Melissa Bowen (UoA) and Robert Smith (UoO)

A dissertation submitted for the degree of

BSc(Hons) in Geophysics

School of Environment

University of Auckland

November 5, 2018

Word count: 11,826

Abstract

This study examines the mean, interannual and decadal variability, and longer-term trends over the altimeter record (September 1992 – May 2017) in the poleward flowing boundary current along the Fiordland coast (referred to as the Fiordland Current, FC). Sea-level anomalies from satellite altimetry were used to calculate across-track geostrophic velocity anomalies. Time-series of possible drivers (South Pacific wind stress curl, southeast Tasman wind stress curl, alongshore wind stress, and the alongshore pressure gradient) were also calculated over the altimeter record. In the mean state, the poleward flow in the FC extended 73.1 km offshore. Spatial structure was evident in the FC, with a stronger inner current and weaker outer current. Examination of the alongshore momentum balance suggests that the mean flow in the FC is driven by the poleward-sloping alongshore pressure gradient, which is larger than the equatorward alongshore wind stress. At interannual time-scales, variability in the FC was positively correlated with the alongshore wind stress ($r = 0.30$, $p < 0.05$), indicating that an equatorward (poleward) alongshore wind stress drives an equatorward (poleward) velocity anomaly. However, this correlation was not strong and so it is hypothesised that multiple factors may contribute toward interannual variability in the FC. At decadal time-scales, variability in the FC was positively correlated with the South Pacific wind stress curl ($r = 0.62$, $p < 0.05$) indicating that as the South Pacific wind stress curl increases (decreases), the poleward flow in the FC weakens (strengthens). Over the long-term record (1993 – 2016) the outer current showed a weakening trend. Both the long-term trend and decadal signal are consistent with the response of a traditional eastern boundary current to spin-up of the South Pacific subtropical gyre. In contrast, the inner current strengthened over the altimeter record, suggesting that different dynamics may be forcing the inner FC. The increasing trend in the inner current may result in increased poleward transport of subtropical water, with potential impacts for the regional oceanography and marine ecosystems around southern New Zealand.

Contents

List of Figures

List of Tables

1 Introduction

The boundary current off the west coast of Fiordland, southwest New Zealand, is a narrow, poleward flowing current located close to the coast [Heath 1973]. This current provides a pathway for the outflow of subtropical water (STW) from the southeastern Tasman Sea, and is part of the anticlockwise flow around southern New Zealand [Brodie 1960; Heath 1973, 1975; Chiswell et al. 2015]. Because of this, it likely contributes to the regional transport of heat, salt, nutrients and larvae. The current is also likely part of the Southern Hemisphere 'supergyre', the interconnected gyre that links the South Pacific, Indian, and South Atlantic subtropical gyres [Speich et al. 2002; Cai 2006; Ridgway and Dunn 2007]. As such, it may contribute to the warm surface water route of the Meridional Overturning Circulation (MOC), which ultimately returns surface waters to the North Atlantic [Ridgway and Dunn 2007; Speich et al. 2007].

Increased transport of STW around southern New Zealand, as anticipated under increased wind stress curl (WSC), may lead to an increase in water temperatures to the south of New Zealand [Cortese et al. 2013; Shears and Bowen 2017]. This increased transport may result in a change in the proportion of STW being transported northward along the southeast coast of New Zealand via the Southland Current (SC), which transports predominantly subantarctic water (SAW) [Sutton 2003]. Changes in the southward transport of STW in the Fiordland boundary current may also influence the position of the subtropical front (STF) around southern New Zealand [Hamilton 2006; Smith et al. 2013]. These changes may impact on the marine ecology of the region [Shears and Bowen 2017], as has been seen to occur with poleward expansions in the range of tropical and subtropical species associated with increased southward penetration of the East Australian Current (EAC) [e.g. Ling et al. 2009; Fowler et al. 2017]. However, despite the possible importance of this boundary current to the regional oceanography and marine ecosystems, little is known about its variability or long-term trend.

This introduction will give an overview of the regional Tasman Sea oceanography (section 1.1), introduce the theory of eastern boundary currents (EBCs) (section 1.2), and identify the EBCs of the Tasman Sea (section 1.3). Variability and trends identified in other New Zealand boundary currents will be outlined (section 1.4), and finally the aims of the study will be presented (section 1.5).

1.1 Regional Oceanography

The Tasman Sea is located between Australia and New Zealand and is bounded to the north by the Tasman Front (TF) and to the south by the STF (Fig. 1). The TF is a band of eastward flowing STW, formed where the EAC, the western boundary current (WBC) of the South Pacific subtropical gyre, separates from the Australian coast between approximately 31–34° S [Ridgway and Dunn 2003]. The TF is one of the main outflows from the Tasman Sea [Sutton and Bowen 2014], with part of the flow in the EAC travelling eastward in the TF, and part continuing south along the east Australian coast into the Tasman Sea as the EAC extension (EACx) [Ridgway and Dunn 2003; Ridgway 2007]. Ridgway and Dunn [2003] gave a mean transport of 19.2 Sv in the EACx and 12.9 Sv in the TF. More recently, Sutton and Bowen [2014] found the mean transport in the TF to be 7.8 Sv. Hill et al. [2011] found that transport in these two pathways are anti-correlated on decadal time scales.

Water also flows out of the Tasman Sea via the Tasman Outflow (TO, Fig. 1), which is also commonly referred to as the Tasman Leakage. The TO is the westward flow of thermocline waters between Tasmania and the Antarctic Circumpolar Current into the Indian Ocean [Ridgway and Dunn 2007; van Sebille et al. 2012]. It is fed by flow from the EACx that turns westward around southern Tasmania [Rintoul and Sokolov 2001]. van Sebille et al. [2012] estimated a mean transport of 4.2 Sv in the TO from ocean simulations. This flow acts as a South Pacific-Indian Ocean connection, allowing Subantarctic Mode Water and Antarctic Intermediate Water to be distributed between ocean basins, and thus is believed to an important part of the global MOC [Speich et al. 2002; Ridgway and Dunn 2007; Speich et al. 2007]. The MOC is the mechanism through which the ocean redistributes heat between the tropics and high latitudes, and thus is important for regulating climate [Gordon 1996; Speich et al. 2002, 2007]. The TO is much less studied than the other upper ocean pathways in the MOC (the Drake Passage and Indonesian Throughflow (ITF)) [Speich et al. 2001; Talley et al. 2011; van Sebille et al. 2012]. It also forms part of the Southern Hemisphere supergyre, which links the South Pacific, Indian, and South Atlantic subtropical gyres [Speich et al. 2002; Cai 2006; Ridgway and Dunn 2007]. This supergyre is an important surface route in the MOC as it ultimately serves to transport Southern Hemisphere waters back to the Atlantic Ocean [Ridgway and Dunn 2007; Speich et al. 2007]. There is large variability in the transport of the TO on both sub-weekly and interannual time-scales [van Sebille et al. 2012] and its strength is related to the regional WSC, with Rintoul and Sokolov [2001] finding that a poleward shift of the zero WSC south of

Tasmania corresponded to a larger TO transport. However, van Sebille et al. [2012] found no trends in the TO over the 1983–1997 period.

The STF separates STW to the north from SAW to the south [Stramma et al. 1995; Hamilton 2006]. In the southern Tasman Sea, the STF is evident as a 400–500 km wide Subtropical Frontal Zone (STFZ) that is enclosed by a northern STF (N-STF), which marks the northward limit of subantarctic surface water, and a southern STF (S-STF), which marks the poleward extent of subsurface STW [Hamilton 2006; Smith et al. 2013]. The S-STF is the main front of the STFZ around New Zealand [Hamilton 2006; Smith et al. 2013]. As the S-STF encounters the New Zealand continental shelf, it is deflected southwards [Sutton 2003; Smith et al. 2013]. This poleward deflection around New Zealand may be reinforced by the poleward flow of STW along the west coast via the Fiordland boundary current [Hamilton 2006; Smith et al. 2013]. There is a weak eastward geostrophic transport of around 3 Sv in the vicinity of the STF [Stramma et al. 1995; Ridgway and Dunn 2003], which, upon reaching the west coast of the South Island, separates into northward (the Westland Current, WC) and southward (the focus of this study) flowing currents at around 41–44° S (Fig. 1) [Heath 1973, 1975; Stanton 1976; Heath 1982, 1985; Stanton and Moore 1992].

The poleward flowing boundary current off Fiordland, which is the focus of this study, is thought to provide a third outflow of water from the Tasman Sea, and may contribute to the return flow of the Southern Hemisphere supergyre. For example, Ridgway and Dunn [2007] show a return flow of the supergyre flowing around the Campbell Plateau; however, they acknowledge that the shallowness of the plateau results in them using a best guess trajectory for the circulation of the supergyre in this region. The circulation of the supergyre in this region is therefore still relatively unknown [Speich et al. 2007].

1.2 Eastern Boundary Currents (EBCs)

Currents on the west coast of New Zealand are EBCs, as they are located on the eastern margin of the Tasman Sea. EBCs tend to be forced by the wind and located in regions of equatorward flowing winds, which drive an offshore Ekman transport [Gill 1982; Talley et al. 2011]. This results in upwelling along the coast, which alters the pressure field as less dense surface waters are transported offshore and denser waters are upwelled to replace them [Gill 1982]. This sets up an equatorward flowing alongshore geostrophic current, which is referred to as an EBC [Talley et al. 2011]. This mechanism can produce EBCs over a larger region than just that experiencing

the local forcing, as the raised thermocline can be propagated poleward by coastally trapped waves (CTWs) [Gill 1982]. Associated with surface EBCs is a poleward flowing undercurrent, often around 200 m deep [Talley et al. 2011]. When the upwelling favourable winds stop, this poleward undercurrent can extend to the sea-surface [Talley et al. 2011].

EBCs tend to flow from high to low latitudes [Gill 1982; Talley et al. 2011], however not all EBCs do so. For example, a freshwater plume entering the ocean on an eastern boundary tends to be deflected poleward by the Coriolis force, and freshwater inflow can also set up a buoyancy-forced poleward-flowing EBC [Gill 1982]. Similarly, a poleward alongshore wind stress creates an onshore Ekman transport, raising the sea surface near the coast, resulting in a cross-shelf pressure gradient which drives a poleward-flowing geostrophic EBC [Talley et al. 2011]. A well-studied example of an anomalous, poleward-flowing EBC is the Leeuwin Current (LC), which is the EBC of the Indian Ocean [Talley et al. 2011]. The LC flows poleward along the west Australian coast, against the prevailing equatorward flowing winds, and is driven by a strong alongshore pressure gradient arising from the warm-water pool created by the ITF [Godfrey and Ridgway 1985; Morrow and Birol 1998; Feng et al. 2003; Ridgway and Condie 2004; Talley et al. 2011]. This alongshore pressure gradient is large for an eastern boundary, and of similar magnitude to those which drive the poleward flowing WBCs [Godfrey and Ridgway 1985]. Seasonal variability in the LC is driven by the northward alongshore wind stress, with the current strongest when the northward alongshore wind stress is weakest [Smith et al. 1991; Feng et al. 2003]. This results in a weaker LC in the austral summer, when the prevailing southerly winds are stronger, and a stronger LC in the austral winter, when then the prevailing southerly winds are weaker [Godfrey and Ridgway 1985; Feng et al. 2003]. Morrow and Birol [1998] also found that the alongshore pressure gradient was at a maximum when the LC was strongest, suggesting that variability in the pressure gradient also drives variability in the LC. Interannual variability in the LC is dominated by the El Nino-Southern Oscillation (ENSO), with the LC stronger during a La Nina event and weaker during an El Nino [Feng et al. 2003].

1.3 New Zealand EBCs

The EBCs of the Tasman Sea are the West Auckland Current (WAuC), WC, d'Urville Current (dUC), and (depending on the literature) the SC (Fig. 1). The WAuC was originally described by Brodie [1960] as a southward flowing current down the west coast of Northland. However, in a more recent study, Sutton and Bowen [2011] found a southeastward tendency of the flow

offshore of the 1000 m isobath and a weaker northward tendency of the inshore flow, concluding that the area contained weak flows dominated by variability. Further south, the dUC flows eastwards from the western side of Cook Strait into the strait, and is fed by the WC [Brodie 1960; Chiswell et al. 2015]. The WC flows northeastwards along the west coast of the South Island and is driven by the prevailing southwesterly winds [Brodie 1960; Stanton 1976; Heath 1982; Stanton and Moore 1992]. During upwelling conditions, a poleward flowing undercurrent can develop [Stanton and Moore 1992], and when the prevailing winds weaken or disappear, a weak southwestward flowing coastal counter-current can occur [Stanton 1976; Heath 1982]. Further south lies the southwestward flowing geostrophic current that is the focus of this study [Brodie 1960; Stanton 1976; Heath 1973; Stanton and Moore 1992; Moore and Murdoch 1993]. As a comparison with the LC, this current is also a poleward-flowing EBC that is believed to be driven by a poleward-sloping pressure gradient that opposes the prevailing winds [Stanton 1976; Ridgway and Dunn 2003]. It was therefore suggested by Ridgway and Dunn [2003] that this current may exhibit dynamics similar to the LC.

The extent to which this current on the Fiordland coast is connected to the SC on the east coast of the South Island is not entirely clear, as the SC has historically referred to two different geographic extents of flow. In an early study of New Zealand coastal currents, Brodie [1960] considered the current flowing southwestward along the Fiordland region of the west coast, eastwards through Foveaux Strait, and then northeastward up the east coast of the South Island as the SC. Heath [1975] also concluded that (mainly) STW flowed southwest along the Fiordland coast, eastward across the Snares Shelf, then turned and flowed northeastwards along the South Island east coast. Stanton [1976] considered the SC to be fully developed and evident in the geostrophic circulation off the Fiordland coast. He calculated surface geostrophic velocities relative to 500 dbar that exceeded 0.2 $\mathrm{m\,s^{-1}}$ and a volume transport of 3.1 Sv offshore of Milford Sound relative to 1000 dbar. Butler et al. [1992] referred to this current off the Fiordland coast as the SC and found strong geopotential gradients along the coast, with southwestward flows of roughly 0.5 $\mathrm{m\,s^{-1}}$ at a depth of 50 m. Stanton and Moore [1992] also referred to the southwestward flowing current off the west coast as the SC and found surface geostrophic velocities of up to 0.6 $\mathrm{m\,s^{-1}}$ across a survey line offshore of Milford Sound. From the same observation experiment, Cahill et al. [1991] found that the mean flow along the coast measured by a mooring at 55 m depth at Big Bay was 0.05 $\mathrm{m\,s^{-1}}$ for November 1986 – April 1987. Hamilton [2006] also referred to the poleward flowing boundary current off the Fiordland coast as the SC.

However, in more recent literature the SC is usually considered to be of a smaller geographic extent, extending along the upper continental slope southeast of Stewart Island and flowing northeastwards up the east coast of the South Island toward the Chatham Rise (Fig. 1) [Chiswell 1996; Sutton 2003; Cortese et al. 2013; Chiswell et al. 2015]. Chiswell [1996] came to this conclusion due to differences between the water properties in the currents on the east and west coast, with the salinity at 100 dbar off Milford Sound being much higher than any of their measurements in the SC on the east coast, leading to the conclusion that there is likely not a direct link between the currents. Sutton [2003] reported that the SC off the eastern coast of the South Island transports 8.3 Sv of mainly SAW (90%), with STW (10%, or slightly less than 1 Sv) confined to the inshore portion of the current (inshore of the Southland Front, SF).

To distinguish between the current off the Fiordland coast that is the focus of this study and the more contemporary definition of the SC, it is proposed that the current off the Fiordland Coast be named the Fiordland Current (FC), and it will be referred to as such in this study. In any case, a common agreement between both older and more recent studies is that the general circulation around the south of New Zealand is an anticlockwise flow of water southwestwards along the Fiordland coast, eastwards along the south coast, and northeastwards along the Otago coast (Fig. 1) [Brodie 1960; Heath 1973, 1975; Chiswell et al. 2015].

1.4 Variability and Trends in New Zealand Boundary Currents

Variability in the boundary currents around New Zealand has received some attention. A model by Heath [1982] found that currents on the west coast continental shelf were predominantly driven by boundary forcing and local winds. Cahill et al. [1991] found that alongshore currents on the South Island west coast shelf were related to the alongshore wind stress through Cook Strait, which they believed was producing CTWs. They also found that alongshore wind stress along the west coast was producing alongshore currents. Sutton and Bowen [2011] found that variability in the flow offshore of the 1000 m isobath off the West Auckland coast was largely geostrophic, while inshore variability was correlated to changes in wind stress.

On the east coast of New Zealand, Chiswell [1996] found that, over seven months of data collected, variability in the SC was mainly driven by local winds. Hopkins et al. [2010] found evidence of seasonal variability in the strength of the SC, with the sea-surface temperature (SST) gradient across the SF (a proxy for the strength of the geostrophic flow) strongest in the summer and winter, while gradients, and therefore velocity, were weakest in spring. In a study

of New Zealand's WBCs, Fernandez et al. [2018] found that the flow in the Subantarctic Front was in phase with the South Pacific wind stress curl (SPWSC), with greater flow during periods of stronger WSC. Statistically significant seasonal cycles in the East Cape Current (ECC) and SC were also found, likely in response to local winds. The ECC was found to have stronger transport in late summer and weaker transport in early winter, with the local WSC a potential driver of this annual cycle. Transport in the SC was at a maximum in April and minimum in November. In general, Fernandez et al. [2018] concluded that New Zealand WBCs were highly variable, and found no significant trends over the 1993–2014 period.

Little research has been carried out on ENSO-driven variability in New Zealand boundary currents, though studies have suggested that ENSO can have an impact [Stanton 2001; Hopkins et al. 2010; Fernandez et al. 2018]. Fernandez et al. [2018] found little correlation between ENSO and flow in any of the New Zealand WBCs, with the highest correlation in the EAuC. However, even this correlation was not consistent as weaker transports were found during both El Nino and La Nina events. Stanton [2001] also found inconsistencies in the response of the EAuC to ENSO events, with these inconsistencies likely due to different wind anomalies produced by different strength ENSO events. Hopkins et al. [2010] found that variability in the SC on interannual time-scales was correlated with ENSO variability. However these correlations were found to also depend on the season.

To date, little work has been conducted examining variability in the FC. Stanton [1976] believed that the component of the current driven by the predominant southwesterly winds was not strong enough to reverse the southwestward flow of the geostrophic current. This was supported by Stanton and Moore [1992] who found that a southwestward geostrophic current was always present, although a northeastward flowing coastal current developed under northeastward wind stress. Therefore the FC was not always found up against the coast, with the northeastward coastal current likely moving the core of the FC offshore. Cahill et al. [1991] also found, from moorings at roughly 60 m depth, that, while the flow was generally poleward, equatorward velocities occasionally developed. Using moored current meter data offshore of Milford Sound, Chiswell [1996] found that the southwestward flow reversed and became northeastward 36% of the time. However this result came from only one month of data.

From the findings of these studies, variability in the FC might be expected to be predominantly wind-driven, either by local winds, by wind over the greater South Pacific region, or both. If the SPWSC is a key driver, a decadal signal in the FC may be present. For example, Hill et al. [2011] found that decadal variability in the strength of the EACx and TF were related to

decadal variability in the SPWSC, with a maximum WSC associated with maximum transport in the EACx. Fernandez et al. [2018] also found that the SPWSC showed a decadal signal over their 20 year study period.

Longer-term trends in the FC related to long-term changes in the South Pacific winds might also be expected. For example, the EACx extended further south over the approximately 60-year (1944–2002) time period examined by Ridgway [2007], resulting in increased SST and salinity to the east of Tasmania. This increased southward penetration of the EAC is believed to have been caused by a strengthening of the SPWSC over the last half century, which shifts the South Pacific subtropical gyre south and favours transport in the EACx over the TF [Cai 2006; Ridgway 2007; Roemmich et al. 2007; Hill et al. 2008, 2011; Shears and Bowen 2017]. Cai [2006] also found that increases in the Southern Hemisphere mid-latitude WSC have resulted in a spin-up of the Southern Hemisphere supergyre. Future warming of the Tasman Sea, partly driven by an increase in the strength of the EAC, is projected by climate models [Hill et al. 2011; Oliver and Holbrook 2014]. These expected trends are consistent with findings by Cortese et al. [2013], who analysed SST proxies for the period 120k–135k years ago, when global temperatures were 2-3°C warmer. They found that SSTs in the southwest Pacific were warmer than present, hypothesising a stronger EAC transporting STW further south. This was potentially forced by an increase in the SPWSC, causing a spin-up and therefore greater poleward penetration of the subtropical gyre, resembling present-day observations in the Tasman Sea region [Cai et al. 2005; Cai 2006; Hill et al. 2008; Cortese et al. 2013]. Cortese et al. [2013] also found warmer temperatures to the south of New Zealand, which may indicate a stronger FC transporting more STW around the south of New Zealand [Shears and Bowen 2017].

1.5 Aims

The aims of this study are to; a) identify the mean, interannual variability, and longer-term trends in the FC over the altimeter record (the last approximately 25 years), and b) identify potential drivers of the mean, interannual variability, and longer-term trends in the FC. This will be achieved by using sea-level anomaly (SLA) data from the Copernicus Marine Environment Monitoring Service (CMEMS). Differences in SLA can be used to estimate variability in geostrophic currents as differences in SLA create pressure gradients which drive these geostrophic flows [Chelton et al. 2001; Sutton and Bowen 2011; Fernandez et al. 2018]. These variations in geostrophic velocity will be compared to both local and regional winds, to the

alongshore pressure gradient, and to the SOI to determine the extent to which these drive variability in the FC. These comparisons will test possible drivers of variability in this current which a) is a likely pathway for STW transport out of the Tasman Sea, and b) may affect oceanographic conditions and marine ecosystems along the coastline of southern New Zealand.

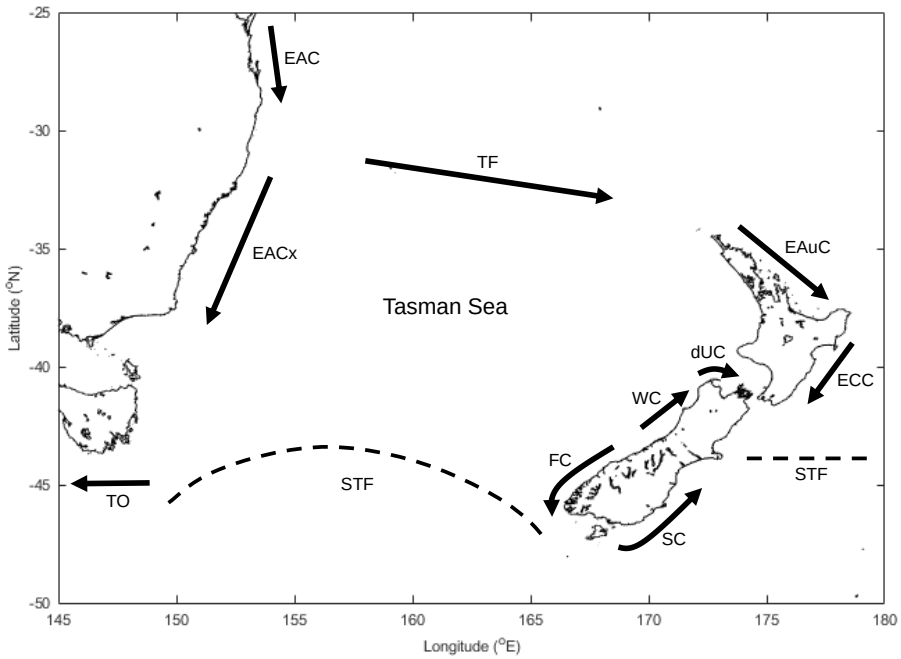

Figure 1: Schematic of the main currents in the New Zealand/Tasman Sea region. Currents are; East Australian Current (EAC), East Australian Current extension (EACx), Tasman Outflow (TO), Tasman Front (TF), East Auckland Current (EAuC), East Cape Current (ECC), Southland Current (SC), Fiordland Current (FC), Westland Current (WC), and d'Urville Current (dUC). The Subtropical Front (STF) is also included. Schematic is based on Hamilton [2006] and Chiswell et al. [2015].

2 Methods

2.1 Sea-level Anomaly (SLA)

2.1.1 Data Processing

SLAs are measured by satellite altimeters, which send microwave pulses to an area of the ocean surface and record the time taken for these pulses to return to the satellite [Chelton et al. 2001]. This time-delay is then used to calculate a number of ocean height variables [Mertz et al. 2018]. Unfiltered 1 Hz (6.19 km) along-track delayed-time SLA data for the 25 September 1992 – 15 May 2017 were used in this study. This product is produced and distributed by CMEMS (http://www.marine.copernicus.eu). Data was collected by the Topex/Poseidon satellite

(25 September 1992 – 24 April 2002), Jason-1 satellite (24 April 2002 – 19 October 2008), OSTM/Jason-2 satellite (19 October 2008 – 25 June 2016), and Jason-3 satellite (25 June 2016 – 15 May 2017). The standard corrections and quality control outlined in Taburet [2018] have been applied to the data. Each satellite passes over the same track every 9.9 days. The SLAs are referenced to the mean sea level over the 1993–2012 period.

SLA measurements from track 36 (Fig. 2) were used to study the FC. As bad data (including measurements over land) were not present in the SLA data [Taburet 2018], the location at which the track crossed the Fiordland coast was estimated by linearly interpolating onto a high-resolution coastline between the closest measurement to the Fiordland coast and the closest measurement to the south coast of New Zealand. This gave a location of 45.5727° S 166.6447° E. Using this location, the innermost altimeter measurement was approximately 11 km offshore, and the outermost altimeter measurement considered was approximately 92 km offshore. In total, 14 altimeter measurements along the track were considered.

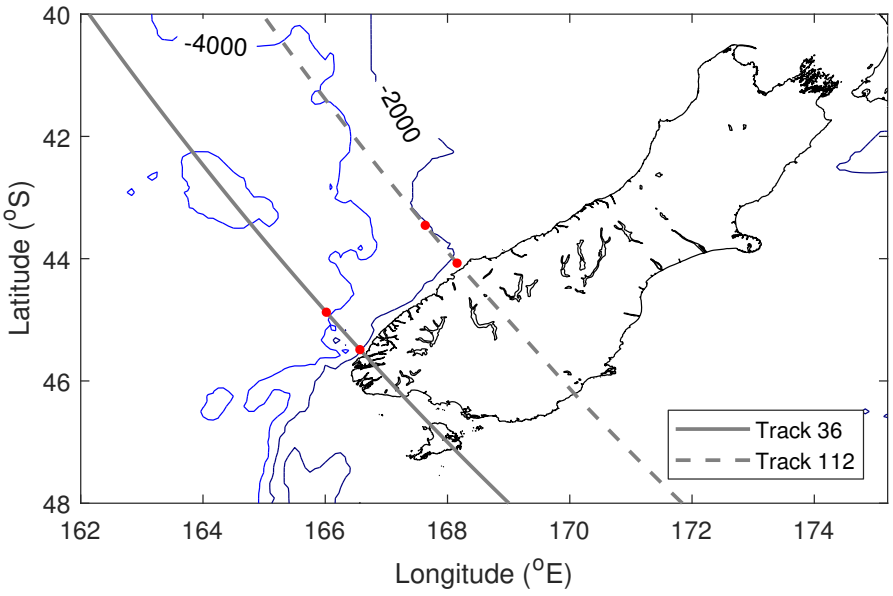

Figure 2: Satellite altimeter tracks 36 and 112. The inner and outer measurements points used in the study are indicated by the red dots. Bathymetric contours are 2000 and 4000 m.

The altimeter data was processed using MATLAB R2017b. First, as missing data was not included in the record, the missing points were found and set as NaNs. Where whole altimeter passes were missing, all 14 measurements for that day were set as NaN. Where altimeter passes occurred over two consecutive days, measurements were combined and the later date used. In total, 10.28% of data points were missing (Fig. A.1). Missing values were infilled by first extrapolating or interpolating smaller gaps in space, and then interpolating in time to fill larger gaps. For the spatial extrapolation, missing data of less than or equal to four measurements

at the ends of the region were infilled through extrapolation by repeating the nearest SLA measurement. This method gave a conservative estimate of the resulting geostrophic velocity anomaly (v_g', see section 2.1.2) as it meant that there was no across-track SLA gradient. For the spatial interpolation, missing data of less than or equal to four measurements within the region (i.e. not at the ends) were infilled through linear interpolation. Up to four missing data points was used for the spatial infilling as the first baroclinic Rossby radius of deformation for the region is between 20–30 km [Chelton et al. 1998]. The gap between good data separated by four missing data points is roughly 30 km and therefore measurements over these spatial scales would be expected to be correlated for geostrophic flows. After the spatial interpolation, any remaining missing data were in gaps consisting of more than four consecutive measurements. This missing data was infilled using a linear interpolation in time.

After infilling, the SLA record was annually smoothed using a cosine filter [Emery and Thomson 2001] to remove higher frequency variability, which was not of interest in the present study. Smoothing was carried out over 39 data points, which corresponds to roughly 390 days (or 13 months).

2.1.2 Geostrophic Velocity

The mean across-track geostrophic velocity ($\overline{v_g}$) for track 36 offshore of the Fiordland coast was calculated using the CNES-CLS13 mean dynamic topography (MDT) and the average unsmoothed SLA, both referenced to 1993–2012, similar to Fernandez et al. [2018]. The CNES-CLS13 MDT was produced by CLS and distributed by Aviso+, with support from CNES (https://www.aviso.altimetry.fr/). SLA was averaged for each measurement location over the full time-series. The MDT was linearly interpolated to the altimeter measurement locations, and the MDT and average SLA at each location were summed to get the average absolute dynamic topography ($\overline{ADT}$). The geostrophic velocity was then calculated by $\overline{v_g} = \frac{g}{f}\frac{\partial \overline{ADT}}{\partial x}$, where g is acceleration due to gravity, f is the Coriolis parameter, and $\frac{\partial \overline{ADT}}{\partial x}$ is the time-averaged along-track ADT gradient with x the distance along the track positive moving onshore. The gradient was calculated using the gradient function in MATLAB, which takes the gradient over three points, except for at the ends where the two adjacent points are used.

The mean geostrophic velocity, $\overline{v_g}$, was used to determine the offshore extent of the FC by noting that the velocity changed sign after the 11th point from the coast, approximately 73.1 km offshore (Fig. 3). Therefore the inshore 11 altimeter measurements were used for the whole

FC. There was also some structure evident in $\overline{v_g}$, with stronger velocities evident closer to the coast and weaker velocities evident further offshore. Due to this structure, changes in the 'inner current' (the inner three points, 11.2–23.6 km offshore) and the 'outer current' (the inner 4–11 points, 29.8–73.1 km offshore) were also examined.

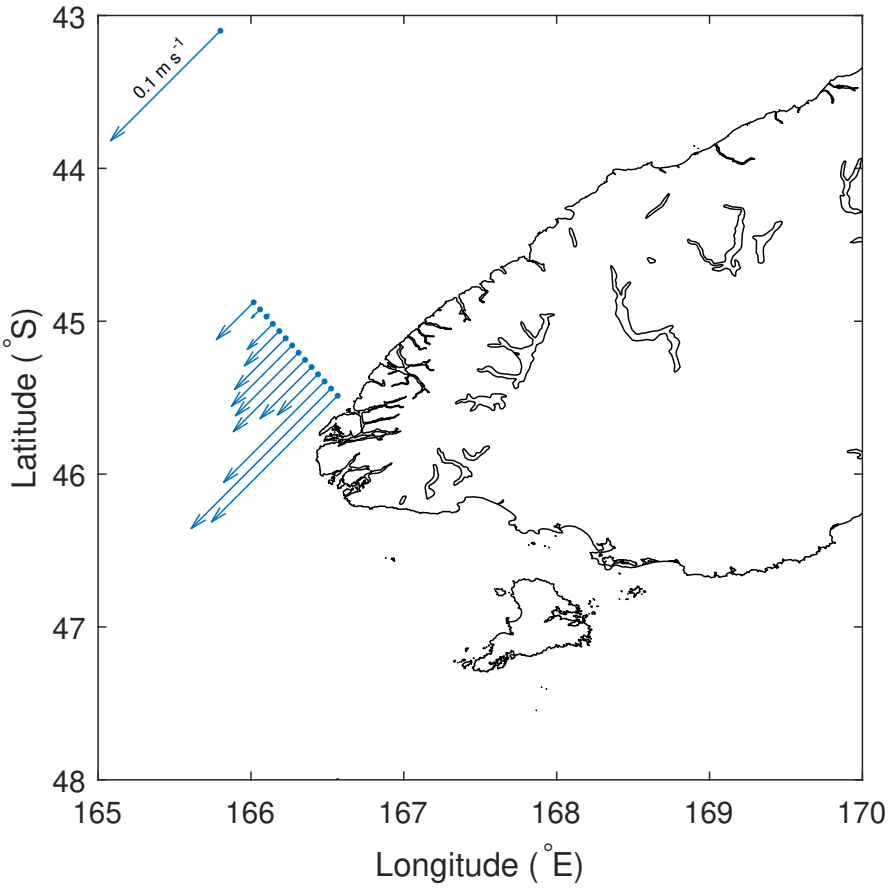

Figure 3: Mean-state across-track surface geostrophic current for October 1992 – May 2017 offshore of the Fiordland coast for altimeter track 36 referenced to the 1993–2012 period. The maximum velocity is 0.13 m s^{-1} southwards. A 0.1 m s^{-1} reference arrow is included in the top left.

A time-series of the across-track surface geostrophic velocity anomaly (v'_g) for track 36 was calculated using the unsmoothed SLA measurements. The velocity anomaly, v'_g, was calculated for each data point from $v'_g = \frac{g}{f}\frac{\partial \eta}{\partial x}$, where $\frac{\partial \eta}{\partial x}$ is the along-track SLA gradient. A positive along-track SLA gradient was defined as sloping down away from the coast (a negative gradient was defined as sloping down toward the coast). A positive velocity was therefore in the northeastward direction along the coast, while a negative velocity was southwestward along the coast. The velocity anomaly, v'_g, at each measurement point was annually smoothed using a cosine filter over 39 data points (13 months). To calculate v'_g over the full FC, the annually-smoothed v'_g was averaged over the 11 inshore measurements for each date. Similarly, annually-smoothed v'_g was averaged over the 3 inshore measurements for the inner current, and over inshore measurements 4–11 for the outer current.

The seasonal cycle and the seasonal anomaly (v'_g minus the seasonal cycle) for the full, inner, and outer currents were also calculated, along with the standard error (SE) of the seasonal cycle. For this, the unsmoothed v'_g was averaged over the 11 inshore measurements for the full current, over the 3 inshore measurements for the inner current, and over inshore measurements 4–11 for the outer current. To calculate the seasonal cycle, the annual average v'_g was removed from each year. The velocity anomaly, v'_g, with the annual average removed, was averaged for each month (i.e. all the January data averaged, all the February data, etc.) to get the seasonal cycle. The seasonal cycle was then removed from the v'_g time-series to obtain the seasonal anomaly. The annually-smoothed seasonal anomaly was calculated by smoothing the seasonal anomaly using a cosine filter over 39 data points (13 months). The SE of the seasonal cycle was calculated for each month from $SE = \frac{SD}{\sqrt{N}}$, where SD is the standard deviation of the month, and N is the number of data points for the month.

Decadal variability has been found in the EACx using five-year smoothed fields [e.g. Ridgway 2007; Ridgway et al. 2008; Hill et al. 2011]. Therefore a time-series was produced to examine decadal variability in the FC by applying a five-year smoothing to the unsmoothed v'_g for the full FC. This smoothing was carried out using a cosine filter over 183 points (61 months).

2.1.3 Alongshore SLA gradient

To examine the influence of the alongshore pressure gradient on the FC, the alongshore SLA gradient between track 36 and track 112 (an altimeter track to the north, Fig. 2) was calculated. To find the alongshore SLA gradient, the SLA data for track 112 was processed and infilled in the same way that the data for track 36 had been, using 44.1607° S 168.2318° E as the location at which the track crosses the Fiordland coast. In total, 8.75% of SLA data was missing for track 112 (Fig. A.2). The mean geostrophic velocity, $\overline{v_g}$, for track 112 was then calculated using the CNES-CLS13 MDT and average SLA in the same way that it was calculated for track 36. From the mean geostrophic velocity, $\overline{v_g}$ (Fig. A.3), it was evident that southwestward velocities extended out to approximately 61.0 km offshore (9 inshore measurements). The inner and outer current spatial structure was also evident at track 112, corresponding to the 3 inshore measurements and inshore measurements 4–9 respectively, though the structure was not as clear as it was at track 36.

To calculate the alongshore SLA gradient, the annually-smoothed track 112 SLAs were linearly interpolated to the same times as the annually-smoothed track 36 SLAs. Average SLAs for the

FC at track 36 were then calculated for each date by averaging the annually-smoothed SLA over the inshore 11 points, inshore 3 points, and inshore points 4–11 for the full, inner, and outer current respectively. For track 112, the inshore 9 points, inshore 3 points, and inshore 4–9 points at each date were used for the full, inner, and outer current respectively. Alongshore SLA gradients for the full, inner, and outer current were then calculated by subtracting the SLA at track 36 from the SLA at track 112, and dividing this by the distance between the altimeter tracks. The negative of these alongshore SLA gradients was taken so that a negative value corresponded to a southwestward-sloping SLA gradient, which would be expected to set up a southwestward (negative) v'_g.

2.2 Wind

Monthly zonal and meridional wind stress data for January 1958 – May 2018 were downloaded from the Japanese 55-year Reanalysis (JRA-55) [Kobayashi et al. 2015].

To examine potential connections between the flow and the large-scale winds, the SPWSC was calculated for the region 20–50° S 180–280° E [e.g. Hill et al. 2008, 2011; Shears and Bowen 2017]. The SPWSC was annually-smoothed using a cosine filter over 13 data points (13 months).

To examine the influence of a more local WSC, the southeast Tasman WSC was calculated for the region 40–45° S 155–165° E. This WSC was annually-smoothed using a cosine filter over 13 data points (13 months).

To examine the influence of local wind stress, the alongshore wind stress along the Fiordland coast was calculated by averaging the wind stress in the region between 44–46° S. At the south of this region the zonal boundaries were 165–166.45° E, and at the north they were 165–168.53° E. The wind stress was then projected (using a scalar projection) onto a straight-line estimate of the Fiordland coast between 45.6767° S 166.5038° E and 44.9529° S 167.1900° E (Fig. A.4) to obtain the alongshore wind stress. The alongshore wind stress was annually smoothed using a cosine filter over 13 data points (13 months).

Decadal variability has been found to occur in the SPWSC [e.g. Hill et al. 2011; Fernandez et al. 2018]. Therefore, to examine the influence of decadal variability in the SPWSC on the FC, a time-series of SPWSC (20–50° S 180–280° E) was calculated with a five-year smoothing using a cosine filter over 61 data points (61 months).

2.3 Correlations

Correlations were calculated between v_g' and potential drivers of the current (alongshore SLA gradient, SPWSC, southeast Tasman WSC, and alongshore wind stress).

To correlate the alongshore SLA gradient with v_g', the annually-smoothed v_g' and annually-smoothed alongshore SLA gradient for the full, inner, and outer current were all detrended. Time-series were detrended so that correlations were of the interannual variability, and were not influenced by longer-term trends. The detrended annually-smoothed negative alongshore SLA gradient for the full current was correlated with the detrended annually-smoothed v_g' for the full current. The negative was taken as the mean flow of the FC is poleward (Fig. 3) and therefore a positive correlation would be calculated between a southwestward-sloping alongshore SLA gradient and a southwestward v_g' (also see section 2.1.3). Likewise, the negative alongshore SLA gradient for the inner and outer currents were correlated with v_g' for the inner and outer currents respectively.

To correlate the wind data (SPWSC, southeast Tasman WSC, alongshore wind stress) with v_g', the annually-smoothed wind time series were linearly interpolated to the same dates as the annually-smoothed v_g'. The annually-smoothed wind data was then detrended and correlated with the annually-smoothed detrended v_g' for the full, inner, and outer current.

The Southern Oscillation Index (SOI) was also correlated with v_g' to determine if there was any correlation between interannual variability in v_g' and interannual variability in ENSO. Following Shears and Bowen [2017], monthly SOI values were downloaded from https://www.esrl.noaa.gov/psd/gcos_wgsp/Timeseries/SOI/, which is based on the methodology given by Ropelewski and Jones [1987]. Values were available from January 1866 – April 2018. The SOI was annually-smoothed using a cosine filter over 13 data points (13 months). The annually-smoothed SOI was then linearly interpolated to the same dates as the annually-smoothed v_g' and detrended. Correlations between the detrended annually-smoothed SOI and the detrended annually-smoothed v_g' were calculated for the full, inner, and outer current.

To evaluate the statistical significance of the correlations, an Effective Degrees of Freedom (EDOF) was calculated for each detrended annually-smoothed time-series by auto-correlating each time-series and finding the time to the first zero crossing of the correlation coefficient (r). The area under the curve to this zero crossing was calculated and the integral time scale, i.e. the time for a curve with perfect correlation (r = 1) to have the same area, was found [Emery

and Thomson 2001]. The EDOF was then found by dividing the length of the time-series by the integral time scale. The smallest EDOF of the two time-series being correlated was used, along with the correlation coefficient (r) between the time series, to calculate the p-value of the correlation. p-values were calculated using a two-tailed t-test from Soper [2018].

Lagged correlations for the detrended annually-smoothed data were also calculated for lags of 1, 2, 3, 4, and 5 years.

To assess links between decadal variability in the FC and SPWSC, correlations were calculated between the detrended five-year smoothed v_g' and the detrended five-year smoothed SPWSC, and the significance of the correlation was evaluated, following the methods above.

2.4 Significance of Linear Trends

95% confidence intervals were calculated to assess the significance of the linear trends for the annually-smoothed v_g' time-series for the full, inner, and outer current, and for the annually-smoothed time-series of the drivers (SPWSC, southeast Tasman WSC, alongshore wind stress, and alongshore SLA gradient for the full, inner, and outer current). Confidence intervals were calculated by $\pm t\frac{s}{\sqrt{\sum (x_i-\overline{x})^2}}$, where t is the t-value corresponding to the Degrees of Freedom (DOF), x_i are the x values (in this case dates), and $\overline{x}$ is the mean of the x values [Draper and Smith 1998]. The SE, s, was calculated by $s = \sqrt{\frac{\sum e_i^2}{DOF-2}}$, where e_i are the residuals. t-values were obtained by referencing a t-table (http://davidmlane.com/hyperstat/t_table.html). For each variable, the DOF was the EDOF calculated in section 2.3 [Emery and Thomson 2001]. A linear trend was considered significant if it did not include 0 within its 95% confidence interval [Draper and Smith 1998; Emery and Thomson 2001].

2.5 Relative Magnitudes of the Alongshore Forcing

It has been hypothesised that the FC may be driven by the same forcing factors as the LC (i.e. a poleward-sloping alongshore pressure gradient that opposes the prevailing equatorward alongshore wind) [Ridgway and Dunn 2003]. To determine the relative importance of these forcing factors, an approach adapted from Godfrey and Ridgway [1985] was used. Godfrey and Ridgway [1985] used the depth integral of the alongshore momentum equation to compare the likely roles of the alongshore pressure gradient and alongshore wind stress in driving the LC.

The alongshore momentum equation is

$$\int \frac{Dv}{Dt}\,\mathrm{dz} - R + fU = -g\frac{\partial S}{\partial y} + \frac{\tau}{\rho_0}$$

Where $\frac{D}{Dt}$ is the Lagrangian derivative, R is the depth integral of all Reynolds stress terms, f is the Coriolis parameter, U is the depth integral of u, g is acceleration due to gravity, S is the depth-integrated steric height, y is the alongshore distance, τ is the alongshore wind stress, and ρ_0 is a reference density [Godfrey and Ridgway 1985]. The forcing function of the alongshore flow can be written as $-g\frac{\partial S}{\partial y} + \frac{\tau}{\rho_0}$ (i.e. the right-hand side of the momentum equation). The left-hand side of the equation is not as straightforward, with the alongshore flow in both the acceleration and the integral of the stress, and therefore was not evaluated. The forcing function was used to compare the relative magnitudes of the alongshore pressure gradient and the alongshore wind stress in driving the FC. In the current study, 1028 $\mathrm{kg\,m^{-3}}$ was used as the reference density, and depths of both 100 m (for the surface ocean) and 2000 m (for the full ocean) were used for the depth-integrated steric height. The 2000 m depth was chosen because the measurements for track 112 lay approximately along the 2000 m depth contour (Fig. 2). Furthermore, Heath [1972] found the reference level in the Tasman Basin to be 2300 dbars, but noted that the weak sub-surface flows mean that a shallower reference level should not have a significant effect on surface geostrophic current calculations. For example, Stanton [1976] used a maximum reference level of 1800 dbar off the West Coast of the South Island as this was the maximum depth sampled in his study, though he found similar surface geostrophic velocities for shallower reference levels.

Individual forcing terms (alongshore pressure gradient and alongshore wind stress) and the combined forcing term (sum of the two individual terms) were calculated for both the mean state and for the time-series over the altimeter record for the full, inner, and outer current. To calculate the pressure gradient in the mean state, $\overline{ADT}$ (see section 2.1.2) was multiplied by the depth (either 100 m or 2000 m) and averaged for the full, inner, and outer current as in the alongshore SLA gradient calculation (section 2.1.3). The mean depth-integrated alongshore ADT gradient was then calculated between track 36 and track 112 for the full, inner, and outer current, and this was multiplied by $-g$ to obtain the pressure gradient. Similarly, to calculate the time-varying pressure gradient, the annually-smoothed SLAs along both track 36 and 112 were multiplied by the depth (100 m or 2000 m) and averaged over the full, inner, and outer current at each date. The gradient of the depth-integrated SLA between track 112 and track 36 was calculated for the full, inner, and outer current at each date and this was multiplied by

$-g$ to obtain the pressure gradient. Forcing terms were calculated so that a positive forcing was equatorward (equatorward-sloping alongshore pressure gradient, equatorward alongshore wind stress) and a negative forcing was poleward (poleward-sloping alongshore pressure gradient, poleward alongshore wind stress).

3 Results

3.1 Mean State

The mean across-track geostrophic velocity, $\overline{v_g}$, for the FC (referenced to the 1993–2012 period) was found to be southwestward (poleward) along the Fiordland coast (Fig. 3). A maximum velocity of 0.13 $\mathrm{m\,s^{-1}}$ was found approximately 17.4 km offshore of the coast. The total current extended approximately 73.1 km offshore. As noted previously (section 2.1.2), some spatial structure was evident within the current, with stronger poleward velocities found at the three inshore measurement points (11.2–23.6 km offshore). These inshore points were therefore considered the inner current, with the current from approximately 29.8–73.1 km offshore considered the outer current. The spatially-averaged $\overline{v_g}$ of the mean FC (over the 11 inshore points, from 11.2–73.1 km offshore) was 0.06 $\mathrm{m\,s^{-1}}$ poleward. The mean flow in the inner current was 0.11 $\mathrm{m\,s^{-1}}$ poleward and the mean flow in the outer current was 0.05 $\mathrm{m\,s^{-1}}$ poleward.

3.2 Seasonal Cycle

Seasonal cycles in v_g' were examined for the full, inner, and outer FC (Fig. 4). No clear seasonal cycles were evident in any of the current extents. Further, the magnitude of the seasonal cycle ($-0.019 \pm 0.013 - 0.030 \pm 0.010$ $\mathrm{m\,s^{-1}}$ for the full current, $-0.052 \pm 0.027 - 0.059 \pm 0.028$ $\mathrm{m\,s^{-1}}$ for the inner current, $-0.023 \pm 0.013 - 0.028 \pm 0.011$ $\mathrm{m\,s^{-1}}$ for the outer current) was smaller than the magnitude of the annually-smoothed seasonal anomaly ($-0.064 - 0.067$ $\mathrm{m\,s^{-1}}$ for the full current, $-0.17 - 0.12$ $\mathrm{m\,s^{-1}}$ for the inner current, $-0.067 - 0.84$ $\mathrm{m\,s^{-1}}$ for the outer current). Therefore this study focusses on possible drivers of interannual variability in the FC, rather than on possible drivers of the seasonal cycle.

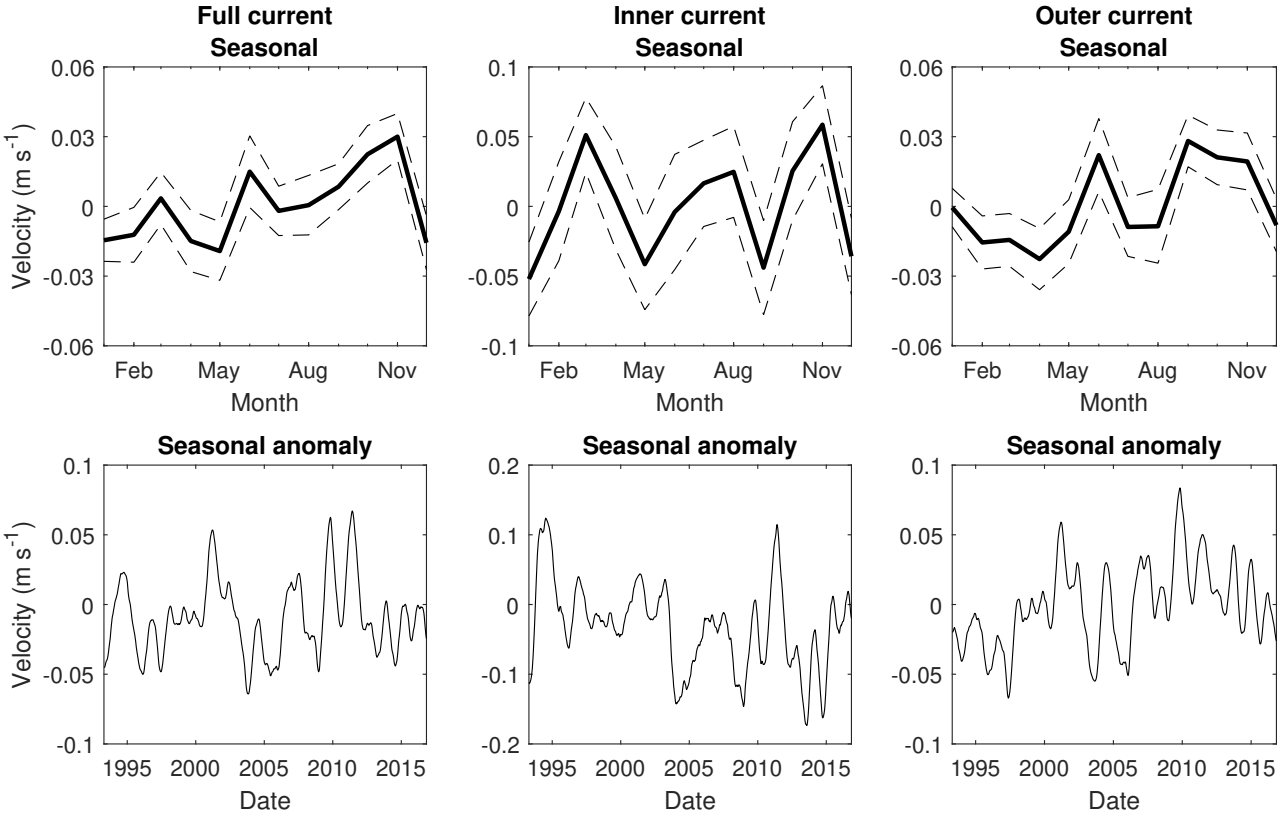

Figure 4: Seasonal cycle (top) and annually-smoothed seasonal anomaly (bottom) of the across-track surface geostrophic velocity anomaly ($\mathrm{m\,s^{-1}}$) for the full Fiordland Current (left), the inner Fiordland Current (middle), and the outer Fiordland Current (right) over the altimeter record (April 1993 – November 2016). Dashed lines on the seasonal cycle are ± 1 standard error. Negative velocities represent a poleward anomaly.

3.3 Interannual Variability

The annually-smoothed time-series of v_g' for the FC were dominated by interannual variability (Fig. 5). Large interannual variability was also evident in possible drivers of the current (Fig. 6 & 7). To investigate the relationship between variability in the FC and these drivers, detrended correlations were calculated (Table 1). The meaning of the sign of the correlations is as follows. A positive correlation between the negative alongshore SLA gradient and v_g' indicates that as the alongshore gradient steepens poleward, the poleward velocity increases. A positive correlation between the SPWSC and v_g' indicates that as the SPWSC increases the poleward velocity decreases. Similarly, a positive correlation between the southeast Tasman WSC and v_g' indicates that as the southeast Tasman WSC increases the poleward velocity decreases. A positive correlation between the alongshore wind stress and v_g' indicates that when the alongshore wind stress is equatorward the poleward velocity decreases. Finally, a positive correlation between the SOI and v_g' indicates that when the SOI is positive the poleward velocity

decreases.

In general, v_g' was weakly correlated ($|r| < 0.3$) with the drivers examined (Table 1). However moderate correlations were found between v_g' over the inner current and the negative alongshore SLA gradient for the inner current ($r = -0.33$), and between v_g' over the full current and the alongshore wind stress ($r = 0.30$). Both these correlations were found to be statistically significant ($p < 0.05$).

Table 1: Correlation coefficients (r), p-values, and Effective Degrees of Freedom (EDOF) for correlations between the detrended, annually-smoothed geostrophic velocity anomaly (for the full, inner, and outer current) and the negative (−ve) of the alongshore sea-level anomaly (SLA) gradient, the South Pacific wind stress curl (S Pacific WSC), the southeast Tasman wind stress curl (SE Tasman WSC), the alongshore wind stress (WS), and the Southern Oscillation Index (SOI). Starred (*) drivers indicate statistically significant correlations.

Driver	**Current**	**r**	**p-value**	**EDOF**
−ve alongshore SLA gradient	Full	0.05	0.750	51
	Inner*	-0.33	0.015	55
	Outer	0.22	0.155	43
S Pacific WSC	Full	0.21	0.255	30
	Inner	0.00	0.990	30
	Outer	0.29	0.122	30
SE Tasman WSC	Full	0.20	0.168	51
	Inner	0.16	0.256	55
	Outer	0.14	0.366	43
Alongshore WS	Full*	0.30	0.030	51
	Inner	0.20	0.138	55
	Outer	0.25	0.106	43
SOI	Full	0.12	0.480	37
	Inner	-0.04	0.816	37
	Outer	0.19	0.250	37

Correlations between annually-smoothed v_g' for the full, inner, and outer FC and its possible drivers were also examined for lags of up to 5 years, with the current lagging the driver (Table 2). In general, lagged correlations were weak ($|r| < 0.3$), although moderate correlations were found with the SPWSC at 3 and 5 year lags, and with the SOI at 1, 3, and 5 year lags. At both 3-year ($r = -0.30$ for the full current, $r = -0.28$ for the inner current, $r = -0.21$ for the outer current) and 5-year ($r = -0.29$ for the full current, $r = -0.34$ for the outer current) lag the SPWSC was negatively correlated with v_g'. The sign of the correlation between the SOI and v_g' varied with the lag, with positive correlations at 1-year lag ($r = 0.31$ for the full current, r

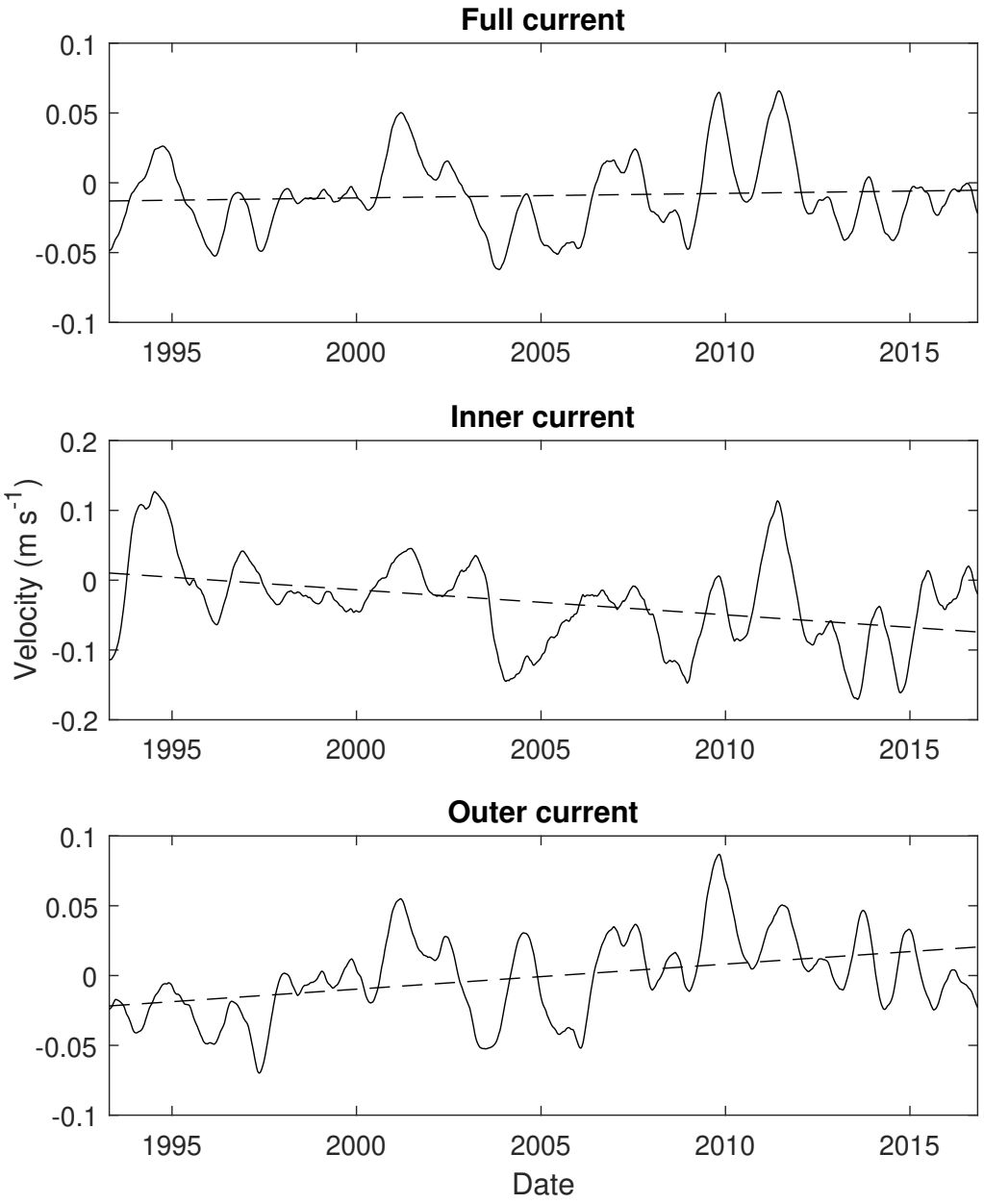

Figure 5: Annually-smoothed, across-track surface geostrophic velocity anomalies ($\mathrm{m\,s^{-1}}$) for the full Fiordland Current (top), inner Fiordland Current (middle), and outer Fiordland Current (bottom) over the altimeter record (April 1993 – November 2016). Dashed lines are the linear trend (full current $= 0.33 \pm 1.11 \times 10^{-2}\,\mathrm{m\,s^{-1}\,decade^{-1}}$, inner current $= -3.59 \pm 2.31 \times 10^{-2}\,\mathrm{m\,s^{-1}\,decade^{-1}}$, outer current $= 1.79 \pm 1.24 \times 10^{-2}\,\mathrm{m\,s^{-1}\,decade^{-1}}$). Negative velocities represent a poleward anomaly.

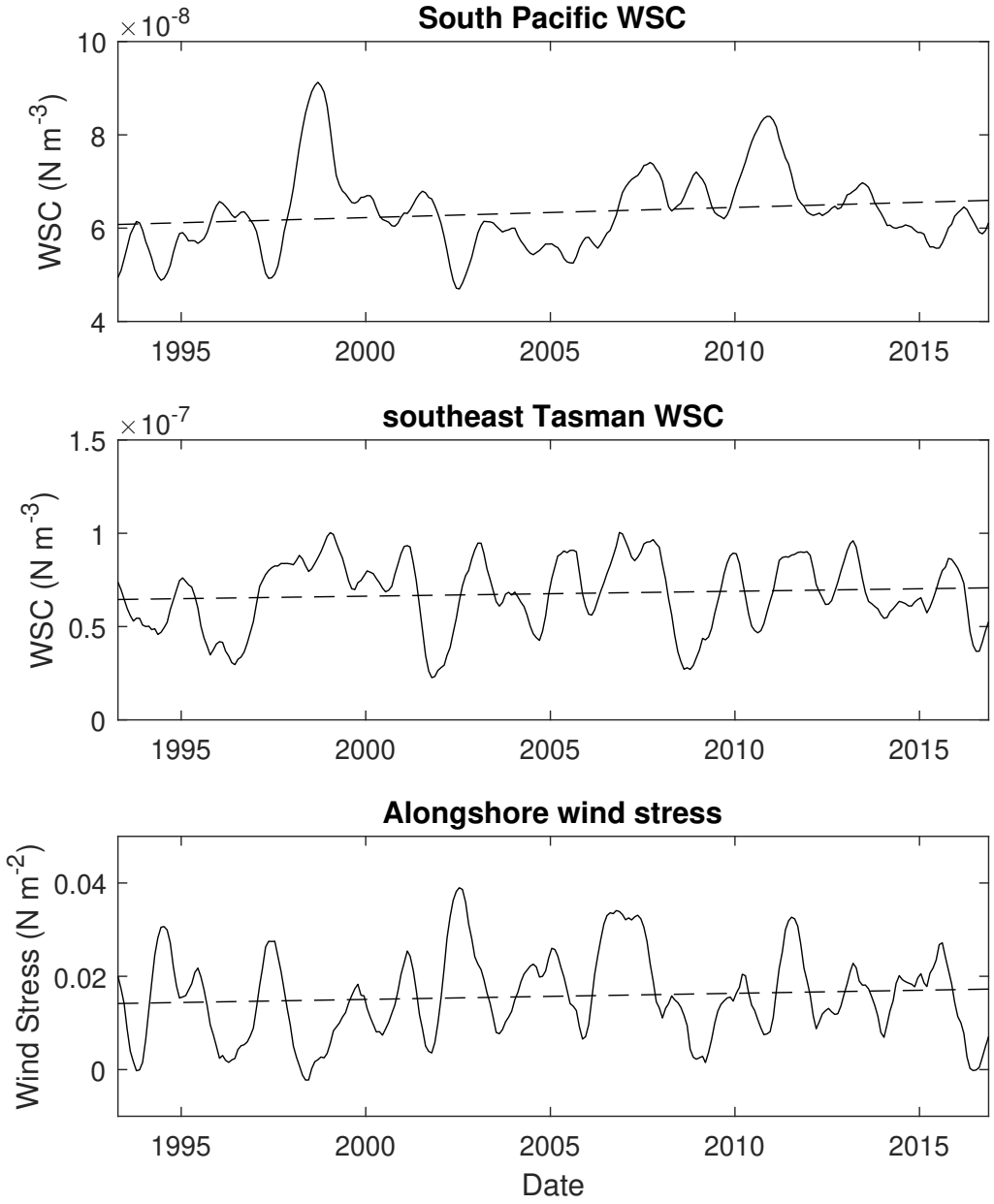

Figure 6: Annually-smoothed South Pacific (180–280° E 20–50° S) wind stress curl (WSC, $\mathrm{N\,m^{-3}}$) (top), southeast Tasman (155–165° E 40–45° S) WSC ($\mathrm{N\,m^{-3}}$) (middle), and alongshore wind stress ($\mathrm{N\,m^{-2}}$, calculated over the region enclosed by 44–46° S with zonal boundaries at 165–166.45° E in the south and 165–168.53° E in the north) (bottom) over the altimeter record (April 1993 – November 2016). Dashed lines are the linear trend (South Pacific WSC $= 2.19 \pm 4.69 \times 10^{-9}$ $\mathrm{N\,m^{-3}\,decade^{-1}}$, southeast Tasman WSC $= 2.65 \pm 7.25 \times 10^{-9}\,\mathrm{N\,m^{-3}\,decade^{-1}}$, alongshore wind stress $= 1.31 \pm 3.33 \times 10^{-3}\,\mathrm{N\,m^{-2}\,decade^{-1}}$). A negative wind stress represents wind flowing poleward along the coast.

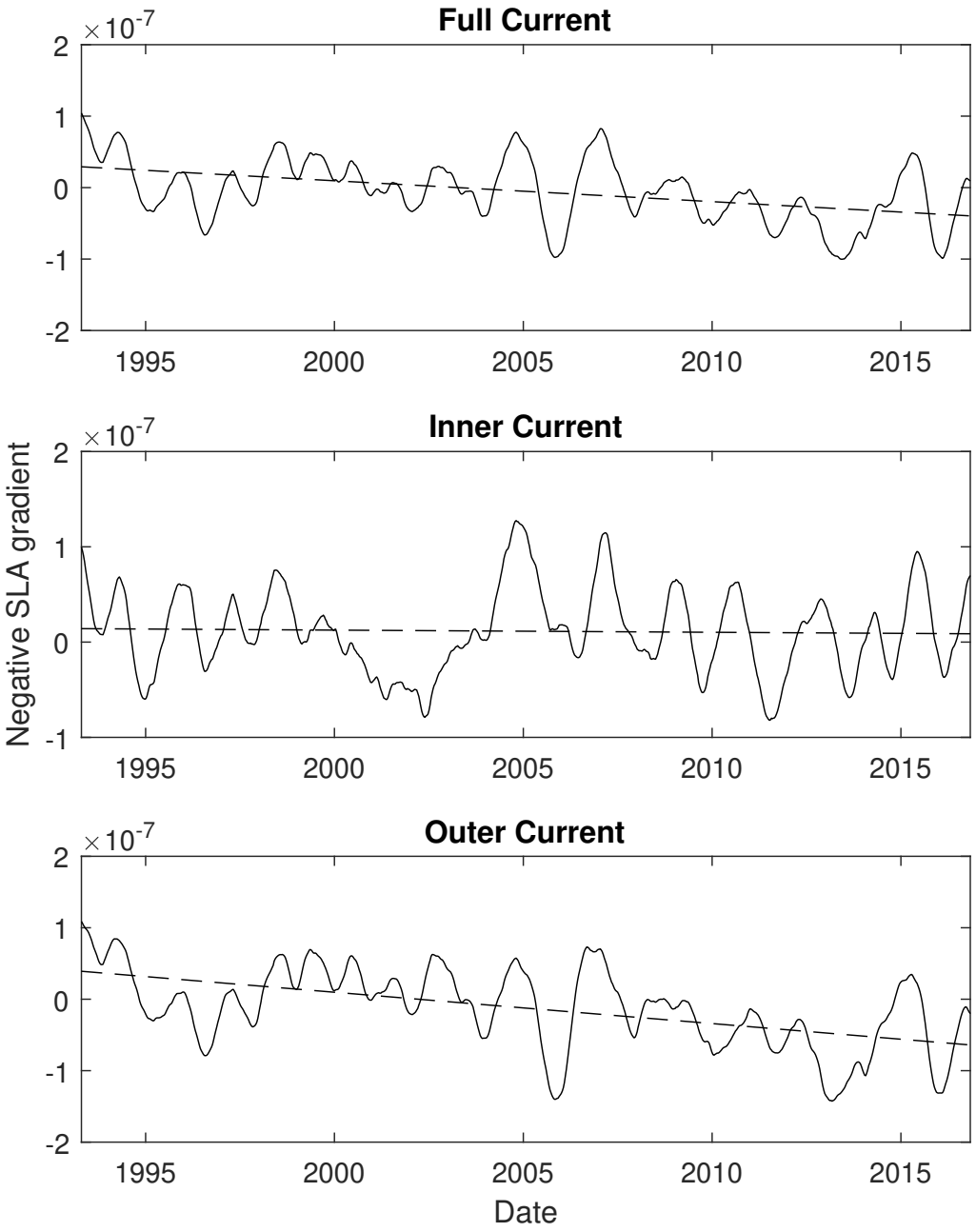

Figure 7: Negative of the annually-smoothed alongshore sea-level anomaly (SLA) gradient between the SLA measurements taken along the northern altimeter track (112) and the southern altimeter track (36) for the full Fiordland Current (top), inner Fiordland Current (middle), and outer Fiordland Current (bottom) over the altimeter record (April 1993 – November 2016). Dashed lines are the linear trend (full current $= -2.92 \pm 1.41 \times 10^{-8}\,\text{decade}^{-1}$, inner current $= -0.23 \pm 1.63 \times 10^{-8}\,\text{decade}^{-1}$, outer current $= -4.38 \pm 1.76 \times 10^{-8}\,\text{decade}^{-1}$). A negative value corresponds to a poleward-sloping alongshore gradient anomaly.

= 0.35 for the outer current) and negative correlations at both 3-year (r = −0.36 for the full current, r = −0.27 for the inner current, r = −0.29 for the outer current) and 5-year (r = −0.30 for the full current, r = −0.44 for the outer current) lags. The statistical significance of the lagged correlations was not evaluated.

Table 2: Correlation coefficients (r) for lagged correlations between the detrended, annually-smoothed geostrophic velocity anomaly (full current, inner current, and outer current) and the negative (−ve) of the alongshore sea-level anomaly (SLA) gradient, the South Pacific wind stress curl (S Pacific WSC), the southeast Tasman wind stress curl (SE Tasman WSC), the alongshore wind stress (WS), and the Southern Oscillation Index (SOI) at lags of 0, 1, 2, 3, 4, and 5 years. For all lags the current lags the driver.

Driver	**Current**	**Lagged Correlation Coefficient (r)**					
		0 yr	1 yr	2 yr	3 yr	4 yr	5 yr
	Full	0.05	-0.21	-0.26	-0.17	0.13	0.02
−ve alongshore SLA gradient	Inner	-0.33	-0.17	-0.18	0.09	0.26	-0.13
	Outer	0.22	-0.11	-0.02	-0.21	-0.09	0.03
	Full	0.21	0.16	-0.08	-0.30	-0.06	-0.29
S Pacific WSC	Inner	0.00	0.10	0.01	-0.28	0.16	-0.09
	Outer	0.29	0.14	-0.12	-0.21	-0.20	-0.34
	Full	0.20	-0.18	-0.09	-0.07	0.00	0.10
SE Tasman WSC	Inner	0.16	-0.20	-0.01	-0.13	0.25	0.07
	Outer	0.14	-0.09	-0.12	0.01	-0.20	0.09
	Full	0.30	-0.11	0.03	0.05	0.07	0.03
Alongshore WS	Inner	0.20	-0.15	-0.14	-0.06	0.09	-0.01
	Outer	0.25	-0.04	0.16	0.12	0.03	0.04
	Full	0.12	0.31	0.11	-0.36	-0.15	-0.30
SOI	Inner	-0.04	0.10	0.12	-0.27	-0.23	0.02
	Outer	0.19	0.35	0.06	-0.29	-0.04	-0.44

3.4 Alongshore Forcing

To compare the relative importance of the alongshore wind stress and alongshore pressure gradient in forcing the FC, the magnitude of these forcing terms was compared. For the mean state (referenced to the 1993–2012 period), the alongshore pressure gradient was the dominant forcing term for both depths of integration considered (100 m and 2000 m, Table 3). Over an integration depth of 100 m the mean pressure gradient forcing was about an order of magnitude larger than the mean alongshore wind forcing ($1.53 \times 10^{-5}\,\mathrm{m^2\,s^{-2}}$) for the full current ($-1.08 \times 10^{-4}\,\mathrm{m^2\,s^{-2}}$) and the outer current ($-1.14 \times 10^{-4}\,\mathrm{m^2\,s^{-2}}$), but not the inner current

($-7.75 \times 10^{-5}\,\mathrm{m^2\,s^{-2}}$, though it was still roughly five times larger here). Using an integration depth of 2000 m, the mean pressure gradient forcing term was found to be two orders of magnitude larger than the mean alongshore wind forcing for all current extents ($-2.17 \times 10^{-3}\,\mathrm{m^2\,s^{-2}}$ for the full current, $-1.55 \times 10^{-3}\,\mathrm{m^2\,s^{-2}}$ for the inner current, $-2.27 \times 10^{-3}\,\mathrm{m^2\,s^{-2}}$ for the outer current). The sign of the forcing terms indicates the direction of the forcing, with the negative alongshore pressure gradient forcing implying a poleward-sloping pressure gradient, while the positive alongshore wind forcing implies an equatorward wind forcing. As the combined forcing is negative, the mean forcing of the FC by these two terms is poleward. This is in agreement with the mean poleward flow observed for the FC (Fig. 3).

Table 3: Average pressure gradient forcing ($\mathrm{m^2\,s^{-2}}$), alongshore wind stress forcing ($\mathrm{m^2\,s^{-2}}$), and the sum of the two ($\mathrm{m^2\,s^{-2}}$) for the full, inner, and outer Fiordland Current over the altimeter record. A negative forcing is poleward.

Current	**Depth Integration (m)**	**Pressure Gradient ($\mathbf{m^2\,s^{-2}}$)**	**Alongshore Wind ($\mathbf{m^2\,s^{-2}}$)**	**Combined Forcing ($\mathbf{m^2\,s^{-2}}$)**
Full	100	-1.08×10^{-4}	1.53×10^{-5}	-9.31×10^{-5}
	2000	-2.17×10^{-3}		-2.15×10^{-3}
Inner	100	-7.75×10^{-5}	1.53×10^{-5}	-6.22×10^{-5}
	2000	-1.55×10^{-3}		-1.53×10^{-3}
Outer	100	-1.14×10^{-4}	1.53×10^{-5}	-9.84×10^{-5}
	2000	-2.27×10^{-3}		-2.26×10^{-3}

Annually-smoothed time-series of both the alongshore pressure gradient anomaly and alongshore wind stress forcing terms were also examined. It was evident that, at interannual timescales, the pressure gradient forcing again dominated for both depths of integration (100 m, Fig. 8, and 2000 m, Fig. A.5). Correlations were not carried out between the annually-smoothed combined forcing time-series and the annually-smoothed v_g' time-series as the alongshore forcing was dominated by the alongshore pressure gradient, and the alongshore SLA gradient had already been correlated with v_g' (Table 1).

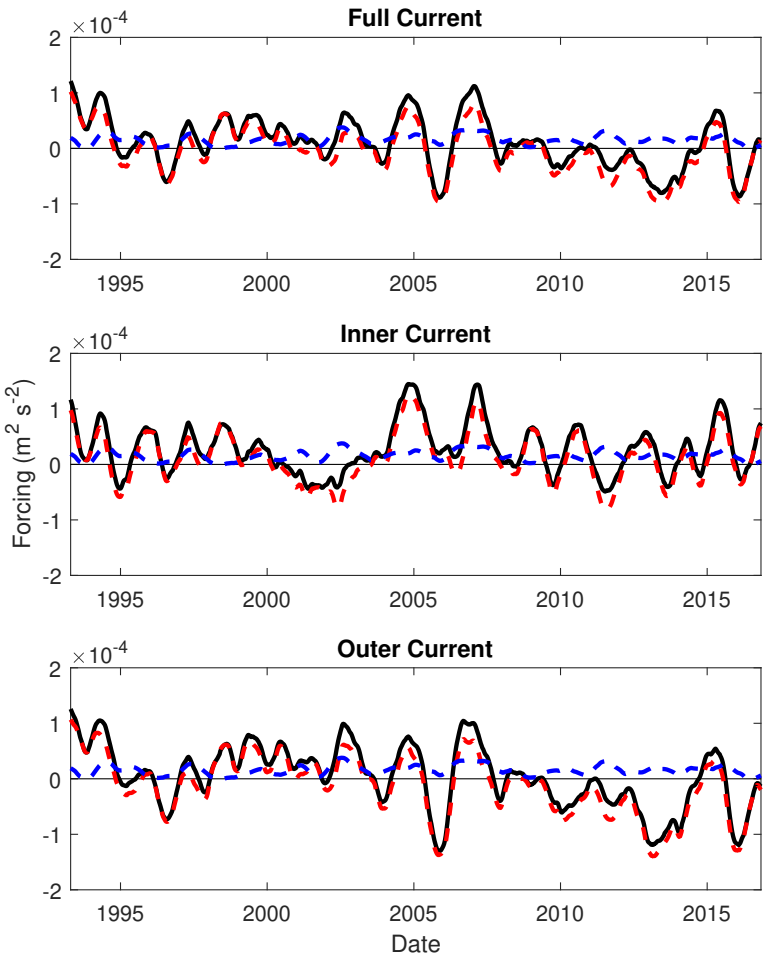

Figure 8: Annually-smoothed alongshore pressure gradient anomaly (red dashed line), alongshore wind stress (blue dashed line), and combined (solid black line) forcing terms ($m^2\,s^{-2}$) integrated over the upper ocean (100 m) for the full (top), inner (middle), and outer (bottom) extents of the Fiordland Current over the altimeter record (April 1993 – November 2016). Negative forcings are poleward.

3.5 Decadal Variability

Decadal variability in the FC was examined by smoothing v_g' for the full FC with a five-year cosine filter. Quasi-decadal variability was evident in the time-series, with maximum positive (equatorward) v_g' in 2001 and 2010 and maximum negative (poleward) v_g' in 1997, 2004, and 2014. The five-year smoothed v_g' was detrended and correlated with the detrended five-year smoothed SPWSC (Fig. 9). A statistically significant positive correlation was found ($r = 0.62$, $p < 0.05$). The positive correlation suggests that when the SPWSC increases, the poleward velocity in the FC weakens. The quasi-decadal cycles appeared to be in phase in the recent time-series, but appeared slightly out-of-phase earlier in the time-series (maximums in the five-year smoothed SPWSC in 1999 and 2010, and minimums in 1992 (not shown), 2004, and 2015).

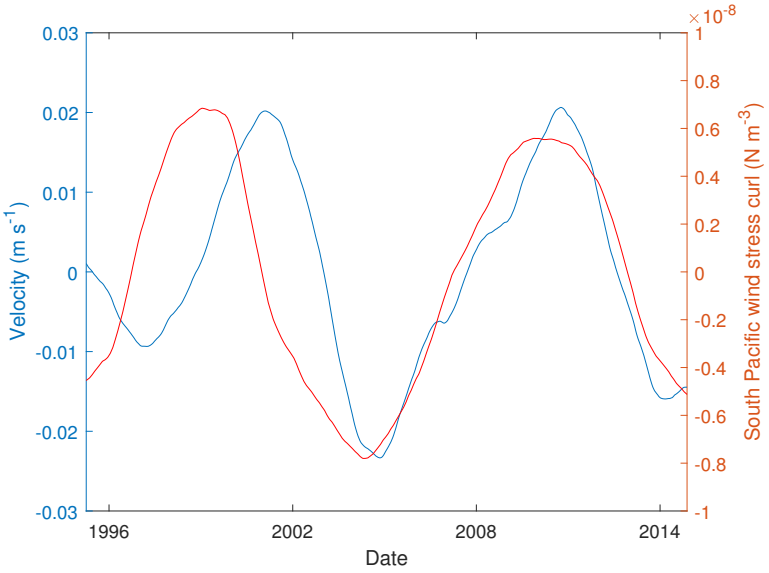

Figure 9: Detrended five-year smoothed across-track surface geostrophic velocity anomaly ($\mathrm{m\,s^{-1}}$) for the full Fiordland Current (blue) and detrended five-year smoothed South Pacific (180–280° E 20–50° S) wind stress curl ($\mathrm{N\,m^{-3}}$, red) over the altimeter record (April 1995 – November 2014). Negative velocities represent a poleward anomaly. The correlation between the time-series is r = 0.62, p = 0.032, EDOF = 12.

3.6 Longer-term Trends

To investigate long-term changes in the flow of the FC, linear trends (with 95% confidence intervals) of the annually-smoothed v_g' were examined (Table 4, Fig 5). No significant trend ($0.33 \pm 1.11 \times 10^{-2}\,\mathrm{m\,s^{-1}\,decade^{-1}}$) was found in the annually-smoothed v_g' for the full extent of the FC. However, statistically significant trends were evident within the current, with a decreasing trend in the inner current ($-3.59 \pm 2.31 \times 10^{-2}\,\mathrm{m\,s^{-1}\,decade^{-1}}$), and an increasing trend in the outer current ($1.79 \pm 1.24 \times 10^{-2}\,\mathrm{m\,s^{-1}\,decade^{-1}}$). As the FC has a mean poleward flow (negative velocity, Fig. 3), these trends indicate that the inner current has strengthened and the outer current weakened over the approximately 23-year record, with the net result being no significant change in the strength of the overall current.

Long-term trends (with 95% confidence intervals) in the annually-smoothed time-series of possible drivers of the FC (SPWSC, southeast Tasman WSC, alongshore wind stress, and alongshore SLA gradient) were also examined (Table 4, Fig. 6 & 7). Over the altimeter record, significant positive trends were only identified in the alongshore SLA gradient for both the full and outer FC, while linear trends in the SPWSC, southeast Tasman WSC, alongshore wind stress, and alongshore SLA gradient for the inner current changed sign within the 95% confidence interval and therefore were not statistically significant.

Table 4: Linear trends in the geostrophic velocity of the Fiordland Current and its potential drivers over the altimeter record (April 1993 – November 2016) with 95% confidence intervals (95% CI). Trends are in units of $\mathrm{m\,s^{-1}\,decade^{-1}}$ for the full geostrophic velocity, inner geostrophic velocity, and outer geostrophic velocity; $\mathrm{N\,m^{-3}\,decade^{-1}}$ for the South Pacific wind stress curl (S Pacific WSC) and southeast Tasman wind stress curl (SE Tasman WSC); $\mathrm{N\,m^{-2}\,decade^{-1}}$ for the alongshore wind stress (Alongshore WS); and $\mathrm{decade^{-1}}$ for the full negative (−ve) alongshore sea-level anomaly (SLA) gradient, inner −ve alongshore SLA gradient, and outer −ve alongshore SLA gradient. Starred (*) variables indicate trends significant at the 95% CI.

Variable	**Trend (decade^{-1})**	**95% CI**
Full geostrophic velocity	0.33×10^{-2}	$\pm\ 1.11 \times 10^{-2}$
Inner geostrophic velocity*	-3.59×10^{-2}	$\pm\ 2.31 \times 10^{-2}$
Outer geostrophic velocity*	1.79×10^{-2}	$\pm\ 1.24 \times 10^{-2}$
S Pacific WSC	2.19×10^{-9}	$\pm\ 4.69 \times 10^{-9}$
SE Tasman WSC	2.65×10^{-9}	$\pm\ 7.25 \times 10^{-9}$
Alongshore WS	1.31×10^{-3}	$\pm\ 3.33 \times 10^{-3}$
Full −ve alongshore SLA gradient*	-2.92×10^{-8}	$\pm\ 1.41 \times 10^{-8}$
Inner −ve alongshore SLA gradient	-0.23×10^{-8}	$\pm\ 1.63 \times 10^{-8}$
Outer −ve alongshore SLA gradient*	-4.38×10^{-8}	$\pm\ 1.76 \times 10^{-8}$

4 Discussion

4.1 Mean Flow

The mean geostrophic flow in the FC was found to be poleward (Fig. 3), as has previously been found along the Fiordland coast [Brodie 1960; Stanton 1976; Heath 1973; Stanton and Moore 1992; Moore and Murdoch 1993]. This mean flow is likely due to the mean poleward-sloping alongshore pressure gradient, which is substantially larger than the mean equatorward alongshore wind stress (Table 3). This result agrees with Ridgway and Dunn [2003], who hypothesised that the FC was driven by the alongshore pressure gradient which opposes the alongshore wind stress. These results also suggest that the mean flow in the FC is primarily driven by the same factors as the mean flow in the LC (i.e. a poleward-sloping alongshore pressure gradient) [Godfrey and Ridgway 1985; Morrow and Birol 1998; Feng et al. 2003; Ridgway and Condie 2004; Talley et al. 2011]. The mean geostrophic velocity structure in the FC, with the strongest velocities near the coast and a general decrease in velocity offshore, is consistent with earlier hydrographic surveys [Heath 1973; Stanton 1976].

4.2 Interannual Variability

Although the mean flow in the FC is likely driven by the alongshore pressure gradient, at interannual time scales variability in both the flow of the FC and in the alongshore pressure gradient are only weakly correlated (Table 1). This is despite the magnitude of the alongshore pressure gradient forcing greatly exceeding the magnitude of the alongshore wind stress forcing at interannual time-scales (Fig. 8). However, a significant correlation was found between interannual variability of the FC and the alongshore wind stress (Table 1). This correlation was positive, indicating that an equatorward (poleward) alongshore wind stress leads to a decreased (increased) poleward velocity in the FC. A possible dynamical explanation of this is that an equatorward alongshore wind stress drives an offshore Ekman transport, lowering sea level at the coast and setting up an onshore sloping pressure gradient. Through geostrophic balance this results in an equatorward alongshore geostrophic velocity [Csanady 1981]. These dynamics are similar to those through which traditional EBCs are set-up [Gill 1982; Talley et al. 2011]. Chiswell [1996] also found that variability in the inshore portion of the SC, which transports mainly STW [Sutton 2003], was strongly correlated to the winds over southern New Zealand. Both of these results therefore suggest that local winds over southern New Zealand may be important in driving variability in STW transport around southern New Zealand.

A significant correlation was also found between interannual variability of v_g' in the inner current and the alongshore SLA gradient for the inner current (Table 1). However this correlation was negative, indicating that as the poleward-sloping gradient weakens (strengthens), the poleward geostrophic velocity increases (decreases). This result is unexpected, with no clear dynamical explanation. It is noted, however, that this result may not be a genuine feature of the dynamics of the FC. It is possible that some error has been introduced by the extrapolation of missing data near the coast, as this is where most of the missing data for track 112 was (Fig. A.2). As both tracks have less missing data later in the time-series (Fig. A.1 & A.2), a comparison of this more recent period would be more robust and is something that could be investigated in the future. A second reason that this result may not reflect the actual driving of variability in the FC is that the alongshore pressure gradient was calculated between two altimeter tracks, and these tracks may be further apart than the scale of the alongshore pressure gradients that drive interannual variability in v_g' at track 36. Stanton [1976] found that the FC strengthens where the continental slope steepens around 44° S (which is roughly the location of the northern altimeter track used here, Fig. 2), whereas it is fully developed further south along the Fiordland coast.

Heath [1975] noted that STW bifurcates into equatorward and poleard flows around 44° S on the West Coast, although the latitudinal range of this bifurcation varies in the literature [Heath 1973, 1975; Stanton and Moore 1992]. The mismatch in scales is also a possible reason why interannual variability in the alongshore pressure gradient is not correlated with interannual variability in the full FC. Furthermore, the innermost measurements along track 112 lie inshore of the 2000 m isobath, while all measurement for track 36 are offshore of this depth, which may impact the alongshore gradient.

Lagged correlations between possible drivers of interannual variability in the FC were also examined (Table 2). Of note here is the negative correlation between the FC and SPWSC at 3 years, and between both the full and outer FC and SPWSC at 5 years. The negative correlation indicates that as the SPWSC increases (decreases), the poleward velocity of the FC increases (decreases). Hill et al. [2008] found that the EAC/EACx was also correlated with the SPWSC at lags of 3 years, with greater transport correlated with a larger SPWSC, although this correlation was found from examining variability on decadal timescales. They proposed that the mechanism causing this lag was barotropic Rossby waves propagating rapidly from the central South Pacific to the eastern coast of New Zealand, where they create a coastal Kelvin wave. This Kelvin wave travels anticyclonically around New Zealand and produces baroclinic Rossby waves along the west coast of New Zealand that take around 3 years to cross the Tasman Sea and influence the EAC [Hill et al. 2010]. This would suggest that it is not the same mechanisms causing the lagged correlations between the FC and SPWSC, and if baroclinic Rossby waves are responsible for the lagged correlation seen here, then these waves would need to be propagating from a region closer to New Zealand [Qiu and Chen 2006; Hill et al. 2008].

The FC was also found to be correlated with the SOI at lags of 1, 3, and 5 years. At 1 year, this correlation was positive, indicating that a negative SOI (i.e. El Nino conditions) was related to increased poleward velocity in the FC. However, at 3 and 5 year lags the correlations were negative, indicating that a negative (positive) SOI was related to reduced (increased) poleward velocity. ENSO was also found to be important for interannual variability in the LC, with a stronger LC during a La Nina year [Feng et al. 2003], the equivalent of a negative correlation here. It is noted that for all drivers, the longer lag correlations may be influenced by the relatively short altimeter time-series in the present study.

Overall, the large interannual variability evident in the FC is consistent with the high interannual variability found by Fernandez et al. [2018] in New Zealand WBCs.

4.3 Decadal Variability

Quasi-decadal variability was present in the FC, and a significant correlation was found between decadal variability in v'_g over the full FC and the SPWSC (Fig. 9). This correlation was positive, which indicates that as the SPWSC increases (decreases), the poleward velocity decreases (increases), which is consistent with the response of a traditional EBC (i.e. increased equatorward transport under a stronger WSC) [Sverdrup 1947]. However the altimeter record may not be long enough for strong conclusions to be drawn about this correlation, as there are only two quasi-decadal cycles present.

Quasi-decadal variability has also been found in the EACx [Ridgway 2007; Hill et al. 2008; Ridgway et al. 2008]. Ridgway [2007] reported that temperature and salinity at Maria Island, Tasmania had a minimum in the mid 1990s then increased to the early 2000s, suggesting a decrease and increase in EACx transport respectively. Consistent with this, Ridgway et al. [2008] observed a weakening of transport in the mid 1990s and a maximum in 2000/2001. In comparison, decadal variability in the FC demonstrated an increased poleward velocity in 1997 and a weaker poleward velocity in 2001, roughly opposing the changes in the strength of the EACx. Fernandez et al. [2018] also found that, in general, weaker surface transports were observed in New Zealand's subtropical WBCs at times of larger SPWSC, consistent with what is seen in the FC. In the case of the New Zealand subtropical WBCs, this weaker transport may be related to reduced transport through the TF [Hill et al. 2011]. However, changes in the transport of the TF would not be expected to directly influence the FC as there is no clear pathway between the two (Fig. 1).

4.4 Longer-term Trends

Significant longer-term trends were evident in the inner and outer FC, with the outer current demonstrating a weakening trend and the inner current demonstrating a strengthening trend (Fig. 5). No significant trend was found in the full FC, consistent with Fernandez et al. [2018] who found no significant trends in the transport of New Zealand WBCs over the altimeter record.

Of the possible drivers considered, significant trends were only present in the alongshore SLA gradient for the full and outer current (Table 4). These trends indicate that the poleward-sloping alongshore gradient has increased (i.e. steepened) over time, however this disagrees

with the weakening poleward velocity trend seen in the outer FC. As has been discussed earlier, this may be because the distance between the altimeter tracks used to calculate the alongshore pressure gradient is at a larger scale than the alongshore pressure gradient that drives the flow in the section of the FC considered here. It is also possible that SLAs in the outer current along track 36 have increased at a slower rate than SLAs in track 112 (which would steepen the alongshore gradient of the outer current) and at a slower rate than SLAs in the inner current of track 36 SLAs (which would steepen the along-track SLA gradient). Steepening of the along-track SLA gradient could lead to an increase in the poleward across-track geostrophic velocity of the inner current, such as has been found here.

The weakening poleward trend in the outer current is consistent with the response of a traditional EBC responding to gyre spin-up due to increased WSC, as has been seen in the South Pacific subtropical gyre [Roemmich et al. 2007, 2016]. However, no significant trend in the SPWSC was found over the altimeter record (Table 4). Other studies [e.g. Hill et al. 2008; Shears and Bowen 2017] have found increasing trends in the SPWSC since the 1950s (and a significant positive trend in the SPWSC was also found in the present study for July 1958 – November 2017, suggesting that the non-significant trend may be due to the short time-series and reduced EDOF). A possible relationship between an increasing SPWSC and weakening poleward flow (increasing equatorward flow) is supported by the correlation between decadal variability in the FC and decadal variability in the SPWSC (Fig 9).

The inner current demonstrates a strengthening poleward trend, opposite to the weakening trend in the outer FC. This suggests that different dynamics may be impacting on the inshore section of the current. Interannual variability and/or the long-term trend in the inner current may be driven by freshwater inflow along the Fiordland coast, with Gill [1982] noting that buoyancy forcing due to freshwater inflow can establish a poleward flowing EBC. An example of where this buoyancy forcing is important in a poleward flowing EBC is in the Norwegian Coastal Current [Mork 1981; Skagseth et al. 2011]. It is possible that freshwater inflow may also be important along the Fiordland coast, as the Fiordland region experiences high rainfall and freshwater runoff [Stanton and Pickard 1981]. Stanton [1976], Butler et al. [1992], and Smith et al. [2013] all found low salinities close to the coast and strong salinity gradients moving offshore for the Fiordland and/or Southland regions.

To briefly examine the relationship between freshwater inflow and the inner FC, monthly rainfall data for Puysegur Point (46.156° S 166.613° E) for January 1991 – June 2018 was downloaded from the New Zealand National Climate Database (https://cliflo.niwa.co.nz/).

This rainfall site was chosen as it was the closest site (74.3 km away) on the Fiordland coast to the innermost altimeter measurement which had a record at least as long as the altimeter record. However, annual rainfall at Puysegur Point is lower than at other locations in Fiordland and may not be representative of the region as a whole [Stanton and Pickard 1981; Tait and Zheng 2007]. Therefore a closer but slightly shorter time-series (January 1994 – January 2018) at Secretary Island (45.221° S 166.886° E), 38.7 km away from the innermost altimeter measurement, was also examined. Missing months were linearly interpolated and annual smoothing, trends, and correlations were calculated using the same methods applied to the altimeter and wind time-series (see Methods, section 2).

Rainfall demonstrated a significant decreasing trend at Secretary Island and a non-significant trend at Puysegur Point (Fig. A.6), suggesting that changes in freshwater inflow may not be driving the long-term changes in the inner current. No correlation ($r = -0.05$, $p = 0.716$) was found between interannual variability in the inner current and Puysegur Point rainfall. A non-significant correlation ($r = -0.13$, $p = 0.388$) was found between interannual variability in the inner current and rainfall at Secretary Island (Fig. A.7). However this correlation was negative, indicating that as rainfall increased (decreased) the poleward geostrophic velocity increased (decreased), as would be expected from a buoyancy driven current [Gill 1982]. Therefore rainfall does not appear to be a significant driver of the inshore FC, although the sign of the correlation at Secretary Island suggests that it may be a contributing factor.

Rainfall is not the only source of freshwater input along the Fiordland coast, with input from rivers (which are fed by both rainfall and snowmelt) and the Manapouri power station tail-race at Doubtful Sound also significant freshwater inputs [Stanton and Pickard 1981]. Importantly, freshwater input from the tail-race is controlled by electricity generating requirements, not rainfall in the Fiordland region [Stanton and Pickard 1981]. Also of note is the substantial spatial variability in rainfall [Tait and Zheng 2007], however both a comparison of rainfall at different locations in Fiordland and an estimate of total freshwater input over the region are beyond the scope of the current study.

4.5 Future Research

The present study has examined the alongshore pressure gradient, SPWSC, southeast Tasman WSC, and alongshore wind stress as possible drivers of interannual variability and long-term trends in the FC, as well as examining the relationship between interannual variability in the FC

and the SOI. The alongshore pressure gradient and alongshore wind stress were also examined as possible drivers of the mean flow in the FC. However other potential drivers exist, such as freshwater buoyancy forcing [Gill 1982]. The alongshore pressure gradient appears to drive the mean flow and should not be ruled out as a driver of interannual variability and long-term trends, despite current relationships suggesting it is not. The lack of a relationship in the present study may be due to the large distance between altimeter tracks used to calculate the alongshore pressure gradient, therefore variability and trends in the pressure gradient over a shorter alongshore distance should be examined. Although this is not currently possible with altimeter data, diagnosing the alongshore momentum balance in numerical simulations would offer some hypotheses about the role of variability in the alongshore pressure gradient. Variability in the FC could also be compared to that in the EAC and/or EACx, as it remains a possibility that some of the STW transported in the EAC exits the Tasman Sea in the FC along the southwest coast of New Zealand [Ridgway and Dunn 2003]. This EAC transport may be particularly important in the inner FC, where an increasing poleward velocity has been observed, as increased poleward transport in the EACx has been observed to occur as the South Pacific gyre spins up [Ridgway 2007; Roemmich et al. 2007].

It could also be worthwhile to make in-situ measurements of the flow in the FC inshore of the altimeter measurements, as it has been noted by Heath [1973], Stanton [1976], and Stanton and Moore [1992] that the flow in the FC is strongest close to the coast, however altimeter measurements are not available for the inshore 11 km. Measurements here may also provide a better method for extrapolating missing inshore altimeter measurements (or verify the method used in this study).

Whilst not specifically related to variability and trends in the FC, it would also be of interest to examine where water transported in the FC ends up. This would help resolve historical discrepancies in the naming of the SC in the literature. It would also have practical benefits by highlighting the areas of the ocean (and coastal New Zealand) affected by changes in the FC. For example, STW flows along the Fiordland coast and around southern New Zealand, with the FC contributing to this. It has been hypothesised that increased transport of STW around southern New Zealand and into the SC has led to SST warming in these regions [Cortese et al. 2013; Shears and Bowen 2017]. If this warming is linked to changes in the FC, it seems reasonable to assume that increased poleward velocity in the inner FC has played an important role. Changes in the transport of STW by the FC could also impact on the marine ecology of southern New Zealand, as has been seen to occur in southeast Australia due to increased

poleward transport of STW in the EACx [e.g. Ling et al. 2009; Fowler et al. 2017]. Increased transport in the inner FC could lead to warming and 'tropicalisation' (i.e. increased proportion of tropical species) around southern New Zealand [Shears and Bowen 2017]. If the FC is found to flow into the SC as expected [Brodie 1960; Heath 1973, 1975], variability and trends in the FC could also be compared with those in the SC, which is more accessible and therefore has been subject to more intensive study than the FC.

5 Conclusions

This study has demonstrated that the mean alongshore flow in the FC is poleward, with the mean current extending approximately 73.1 km offshore. Spatial structure has led to an inner current (11.2–23.6 km offshore) and outer current (29.8–73.1 km offshore) being considered. In the mean, the alongshore momentum equation is dominated by the poleward-sloping alongshore pressure gradient, which is substantially larger than the equatorward alongshore wind stress. It is therefore suggested that the mean poleward flow in the FC is driven by the mean poleward-sloping alongshore pressure gradient.

Large interannual variability was seen in the geostrophic velocity of the FC, however correlations with interannual variability in most of the drivers considered were not statistically significant. A significant correlation was found between the alongshore wind stress and the FC, suggesting that an equatorward (poleward) alongshore wind stress results in reduced (increased) poleward velocity. However, as none of the correlations were strong, it is suggested that the FC may be influenced by a number of factors, with no single driver considered dominant at interannual time-scales.

Decadal variability was also seen in the geostrophic velocity of the FC, and this was significantly correlated with decadal variability in the SPWSC. This correlation indicates that as the SPWSC increases (decreases) the poleward velocity in the FC decreases (increases), which is consistent with the response of a traditional EBC.

Longer-term (1993–2016) trends in the geostrophic velocity of the FC were also found to be statistically significant, with the inner current strengthening and the outer current weakening. The net result was a non-significant trend in the full FC. Trends in the SPWSC, southeast Tasman WSC, and alongshore wind stress were found to not be significant, although the SPWSC demonstrates a significant increasing trend over longer time-periods.

The correlation between decadal variability in the FC and the SPWSC, and the trend in the outer FC are consistent with the dynamics of a traditional EBC and suggest that, on decadal and longer time-scales, a stronger SPWSC may lead to reduced poleward flow in the FC. The trend in the inner FC opposes that of the outer FC and this suggests that the inner current may be controlled by different dynamics, for example buoyancy forcing by freshwater input.

Acknowledgements

I would like to thank my supervisors, Melissa Bowen (University of Auckland) and Rob Smith (University of Otago), for their help and support during my dissertation, it has been immensely appreciated.

The sea-level anomaly (SLA) altimeter products used in this study were produced and distributed by the Copernicus Marine Environment Monitoring Service (CMEMS) (http://www.marine.copernicus.eu). The mean dynamic topography (MDT) product was produced by CLS and distributed by Aviso+, with support from CNES (https://www.aviso.altimetry.fr/). The wind stress data is from the Japanese 55-year Reanalysis (JRA-55) carried out by the Japan Meteorological Agency (JMA). The southern oscillation index (SOI) data is from the Climatic Research Unit, University of East Anglia (CRU), with the data hosted by the National Oceanic and Atmospheric Administation (NOAA) (https://www.esrl.noaa.gov/psd/gcos_wgsp/Timeseries/SOI/). The rainfall data is from the National Institute of Water and Atmospheric Research (NIWA) (https://cliflo.niwa.co.nz/).

References

Brodie, J. W. (1960). Coastal surface currents around New Zealand. *New Zealand Journal of Geology and Geophysics*, 3(2):235–252.

Butler, E. C. V., Butt, J. A., Lindstrom, E., Teldesley, P., Pickmere, S., and Vincent, W. (1992). Oceanography of the Subtropical Convergence Zone around southern New Zealand. *New Zealand Journal of Marine and Freshwater Research*, 26(2):131–154.

Cahill, M. L., Middleton, J. H., and Stanton, B. R. (1991). Coastal-trapped waves on the west coast of South Island, New Zealand. *Journal of Physical Oceanography*, 21:541–557.

Cai, W. (2006). Antarctic ozone depletion causes an intensification of the Southern Ocean super-gyre circulation. *Geophysical Research Letters*, 33:L03712.

Cai, W., Shi, G., Cowan, T., Bi, D., and Ribbe, J. (2005). The response of the Southern Annular Mode, the East Australian Current, and the southern mid-latitude ocean circulation to global warming. *Geophysical Research Letters*, 32:L23706.

Chelton, D. B., deSzoeke, R. A., Schlax, M. G., Naggar, K. E., and Siwertz, N. (1998). Geographical variability of the first baroclinic Rossby radius of deformation. *Journal of Physical Oceanography*, 28:433–460.

Chelton, D. B., Ries, J. C., Haines, B. J., Fu, L.-L., and Callahan, P. S. (2001). Satellite altimetry. In Fu, L.-L. and Cazenave, A., editors, *Satellite Altimetry and Earth Sciences*, volume 69 of *International Geophysics*. Academic Press, San Diego.

Chiswell, S. M. (1996). Variability in the Southland Current, New Zealand. *New Zealand Journal of Marine and Freshwater Research*, 30(1):1–17.

Chiswell, S. M., Bostock, H. C., Sutton, P. J., and Williams, M. J. (2015). Physical oceanography of the deep seas around New Zealand: a review. *New Zealand Journal of Marine and Freshwater Research*, 49(2):286–317.

Cortese, G., Dunbar, G. B., Carter, L., Scott, G., Bostock, H., Bowen, M., Crundwell, M., Hayward, B. W., Howard, W., Martínez, J. I., Moy, A., Neil, H., Sabaa, A., and Sturm, A. (2013). Southwest Pacific Ocean response to a warmer world: Insights from Marine Isotope Stage 5e. *Paleoceanography*, 28:585–598.

Csanady, G. T. (1981). Circulation in the coastal ocean, part 1. *EOS*, 62(2):9–11.

Draper, N. R. and Smith, H. (1998). *Applied Regression Analysis*. John Wiley & Sons, New York, Third edition.

Emery, W. J. and Thomson, R. E. (2001). *Data Analysis Methods in Physical Oceanography*. Elsevier, Amsterdam, 2nd edition.

Feng, M., Meyers, G., Pearce, A., and Wijffels, S. (2003). Annual and interannual variations of the Leeuwin Current at 32°S. *Journal of Geophysical Research*, 108(C11):3355.

Fernandez, D., Bowen, M., and Sutton, P. (2018). Variability, coherence and forcing mechanisms in the New Zealand ocean boundary currents. *Progress in Oceanography*, 165:168–188.

Fowler, A. M., Parkinson, K., and Booth, D. J. (2017). New poleward observations of 30 tropical reef fishes in temperate southeastern Australia. *Marine Biodiversity*.

Gill, A. E. (1982). *Atmosphere-Ocean Dynamics*, volume 30 of *International Geophysics Series*. Academic Press, New York.

Godfrey, J. S. and Ridgway, K. R. (1985). The large-scale environment of the poleward-flowing Leeuwin Current, Western Australia: longshore steric height gradients, wind stresses and geostrophic flow. *Journal of Physical Oceanography*, 15:481–495.

Gordon, A. L. (1996). Communication between oceans. *Nature*, 382:399–400.

Hamilton, L. J. (2006). Structure of the Subtropical Front in the Tasman Sea. *Deep Sea Research I*, 53:1989–2009.

Heath, R. A. (1972). Choice of reference surface for geostrophic currents around New Zealand. *New Zealand Journal of Marine and Freshwater Research*, 6(1-2):148–177.

Heath, R. A. (1973). Direct measurements of coastal currents around southern New Zealand. *New Zealand Journal of Marine and Freshwater Research*, 7(4):331–367.

Heath, R. A. (1975). *Oceanic circulation and hydrology off the southern half of South Island, New Zealand*. New Zealand Oceanographic Institute Memoir 72. New Zealand Department of Scientific and Industrial Research, Wellington.

Heath, R. A. (1982). What drives the mean circulation on the New Zealand west coast continental shelf? *New Zealand Journal of Marine and Freshwater Research*, 16(2):215–226.

Heath, R. A. (1985). Large-scale influence of the New Zealand seafloor topography on western

boundary currents of the South Pacific Ocean. *Australian Journal of Marine and Freshwater Research*, 36:1–14.

Hill, K. L., Rintoul, S. R., Coleman, R., and Ridgway, K. R. (2008). Wind forced low frequency variability of the East Australia Current. *Geophysical Research Letters*, 35:L08602.

Hill, K. L., Rintoul, S. R., Oke, P. R., and Ridgway, K. (2010). Rapid response of the East Australian Current to remote wind forcing: The role of barotropic-baroclinic interactions. *Journal of Marine Research*, 68(3–4):413–431.

Hill, K. L., Rintoul, S. R., Ridgway, K. R., and Oke, P. R. (2011). Decadal changes in the South Pacific western boundary current system revealed in observations and ocean state estimates. *Journal of Geophysical Research*, 116:C01009.

Hopkins, J., Shaw, A., and Challenor, P. (2010). The Southland Front, New Zealand: variability and ENSO correlations. *Continental Shelf Research*, 30:1535–1548.

Kobayashi, S., Ota, Y., Harada, Y., Ebita, A., Moriya, M., Onoda, H., Onogi, K., Kamahori, H., Kobayashi, C., Endo, H., Miyaoka, K., and Takahashi, K. (2015). The JRA-55 reanalysis: General specifications and basic characteristics. *Journal of the Meteorological Society of Japan*, 93:5–48.

Ling, S. D., Johnson, C. R., Ridgway, K., Hobday, A. J., and Haddon, M. (2009). Climate-driven range extension of a sea urchin: inferring future trends by analysis of recent population dynamics. *Global Change Biology*, 15:719–731.

Mertz, F., Pujol, M.-I., and Faugére, Y. (2018). Product user manual for SLA products. *Copernicus Marine Environment Monitoring Service*. [Online]. Available from http://cmems-resources.cls.fr/documents/PUM/CMEMS-SL-PUM-008-032-051.pdf. Accessed 02 March 2018.

Moore, M. I. and Murdoch, R. C. (1993). Physical and biological observations of coastal squirts under nonupwelling conditions. *Journal of Geophysical Research*, 98(C11):20043–20061.

Mork, M. (1981). Circulation phenomena and frontal dynamics of the Norwegian Coastal Current. *Philosophical Transactions of the Royal Society London A*, 302:635–647.

Morrow, R. and Birol, F. (1998). Variability in the southeast Indian Ocean from altimetry: forcing mechanisms for the Leeuwin Current. *Journal of Geophysical Research*, 103(C9):18529–18544.

Oliver, E. C. J. and Holbrook, N. J. (2014). Extending our understanding of South Pacific gyre "spin-up": Modeling the East Australian Current in a future climate. *Journal of Geophysical Research: Oceans*, 119:2788–2805.

Qiu, B. and Chen, S. (2006). Decadal variability in the large-scale sea surface height field of the South Pacific Ocean: Observations and causes. *Journal of physical oceanography*, 36:1751–1762.

Ridgway, K. R. (2007). Long-term trend and decadal variability of the southward penetration of the East Australian Current. *Geophysical Research Letters*, 34:L13613.

Ridgway, K. R., Coleman, R. C., Bailey, R. J., and Sutton, P. (2008). Decadal variability of East Australian Current transport inferred from repeated high-density XBT transects, a CTD survey and satellite altimetry. *Journal of Geophysical Research*, 113:C08039.

Ridgway, K. R. and Condie, S. A. (2004). The 5500-km-long boundary flow off western and southern Australia. *Journal of Geophysical Research*, 109:C04017.

Ridgway, K. R. and Dunn, J. R. (2003). Mesoscale structure of the mean East Australian Current system and its relationship with topography. *Progress in Oceanography*, 56:189–222.

Ridgway, K. R. and Dunn, J. R. (2007). Observational evidence for a Southern Hemisphere oceanic supergyre. *Geophysical Research Letters*, 34:L13612.

Rintoul, S. R. and Sokolov, S. (2001). Baroclinic transport variability of the Antarctic Circumpolar Current south of Australia (WOCE repeat section SR3). *Journal of Geophysical Research: Oceans*, 106(C2):2815–2832.

Roemmich, D., Gilson, J., Davis, R., Sutton, P., Wijffels, S., and Riser, S. (2007). Decadal spinup of the South Pacific subtropical gyre. *Journal of Physical Oceanography*, 37:162–173.

Roemmich, D., Gilson, J., Sutton, P., and Zilberman, N. (2016). Multidecadal change of the South Pacific gyre circulation. *Journal of Physical Oceanography*, 46:1871–1883.

Ropelewski, C. F. and Jones, P. D. (1987). An extension of the Tahiti–Darwin Southern Oscillation Index. *Monthly Weather Review*, 115:2161–2165.

Shears, N. T. and Bowen, M. M. (2017). Half a century of coastal temperature records reveal complex warming trends in western boundary currents. *Scientific Reports*, 7:14527.

Skagseth, O., Drinkwater, K. F., and Terrile, E. (2011). Wind- and buoyancy-induced transport

of the Norwegian Coastal Current in the Barents Sea. *Journal of Geophysical Research*, 116:C08007.

Smith, R. L., Huyer, A., Godfrey, J. S., and Church, J. A. (1991). The Leeuwin Current off Western Australia, 1986–1987. *Journal of Physical Oceanography*, 21:323–345.

Smith, R. O., Vennell, R., Bostock, H. C., and Williams, M. J. (2013). Interaction of the subtropical front with topography around southern New Zealand. *Deep Sea Research I*, 76:13–26.

Soper, D. S. (2018). p-value calculator for correlation coefficients. [Software]. Available from https://www.danielsoper.com/statcalc/calculator.aspx?id=44.

Speich, S., Blanke, B., and Cai, W. (2007). Atlantic meridional overturning circulation and the Southern Hemisphere supergyre. *Geophysical Research Letters*, 34:L23614.

Speich, S., Blanke, B., de Vries, P., Drijfhout, S., Döös, K., Ganachaud, A., and Marsh, R. (2002). Tasman leakage: a new route in the global ocean conveyor belt. *Geophysical Research Letters*, 29(10):1416.

Speich, S., Blanke, B., and Madec, G. (2001). Warm and cold water routes of an OGCM thermohaline conveyor belt. *Geophysical Research Letters*, 28(2):311–314.

Stanton, B. R. (1976). Circulation and hydrology off the west coast of the South Island, New Zealand. *New Zealand Journal of Marine and Freshwater Research*, 10(3):445–467.

Stanton, B. R. (2001). Estimating the East Auckland Current transport from model winds and the Island Rule. *New Zealand Journal of Marine and Freshwater Research*, 35(3):531–540.

Stanton, B. R. and Moore, M. I. (1992). Hydrographic observations during the Tasman boundary experiment off the west coast of South Island, New Zealand. *New Zealand Journal of Marine and Freshwater Research*, 26(3-4):339–358.

Stanton, B. R. and Pickard, G. L. (1981). *Physical Oceanography of the New Zealand Fiords*. New Zealand Oceanographic Institute Memoir 88. New Zealand Department of Scientific and Industrial Research, Wellington.

Stramma, L., Peterson, R. G., and Tomczak, M. (1995). The South Pacific Current. *Journal of Physical Oceanography*, 25:77–91.

Sutton, P. and Bowen, M. (2011). Currents off the west coast of Northland, New Zealand. *New Zealand Journal of Marine and Freshwater Research*, 45(4):609–624.

Sutton, P. J. H. (2003). The Southland Current: a subantarctic current. *New Zealand Journal of Marine and Freshwater Research*, 37(3):645–652.

Sutton, P. J. H. and Bowen, M. (2014). Flows in the Tasman Front south of Norfolk Island. *Journal of Geophysical Research: Oceans*, 119:3041–3053.

Sverdrup, H. U. (1947). Wind-driven currents in a baroclinic ocean; with application to the equatorial currents of the Eastern Pacific. *Proceedings of the National Academy of Sciences*, 33(11):318–326.

Taburet, G. (2018). Quality information document sea level TAC-DUACS products. *Copernicus Marine Environment Monitoring Service*. [Online]. Available from http://cmems-resources.cls.fr/documents/QUID/CMEMS-SL-QUID-008-032-051.pdf. Accessed 03 May 2018.

Tait, A. and Zheng, X. (2007). Analysis of the spatial interpolation error associated with maps of median annual climate variables. *National Institute of Water and Atmospheric Research*. [Online]. Available from https://www.niwa.co.nz/sites/niwa.co.nz/files/import/attachments/Climate_Maps_Error_Analysis.pdf. Accessed 17 October 2018.

Talley, L. D., Pickard, G. L., Emery, W. J., and Swift, J. H. (2011). *Descriptive Physical Oceanography: An Introduction*. Academic Press, Boston, Sixth edition.

van Sebille, E., England, M. H., Zika, J. D., and Sloyan, B. M. (2012). Tasman leakage in a fine-resolution ocean model. *Geophysical Research Letters*, 39:L06601.

A Appendix

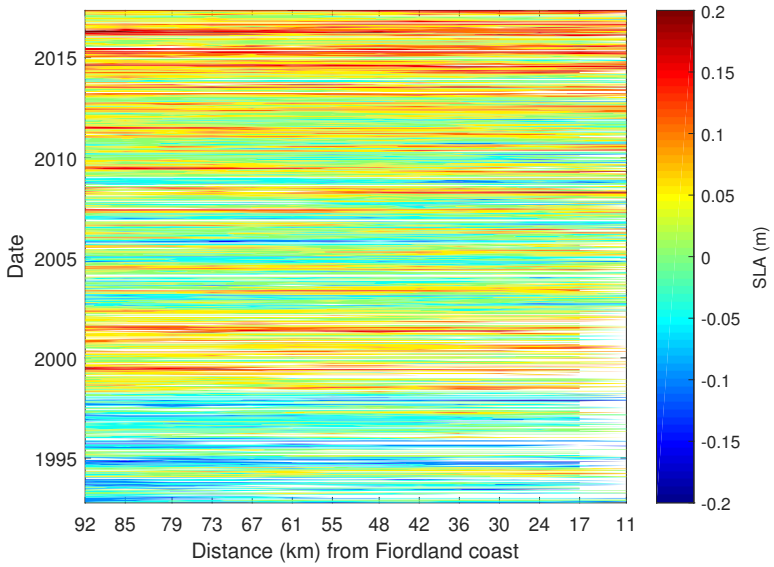

Figure A.1: Hovmöller plot of the sea-level anomaly (SLA, m) along altimeter track 36 offshore (rounded to the nearest km) of the Fiordland Coast for the altimeter record (September 1992 – May 2017). White gaps represent missing data.

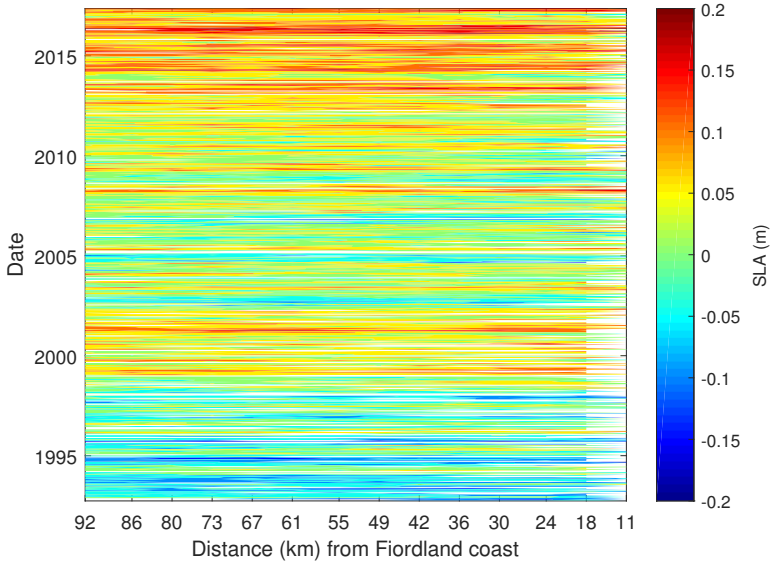

Figure A.2: Hovmöller plot of the sea-level anomaly (SLA, m) along altimeter track 112 offshore (rounded to the nearest km) of the Fiordland Coast for the altimeter record (September 1992 – May 2017). White gaps represent missing data.

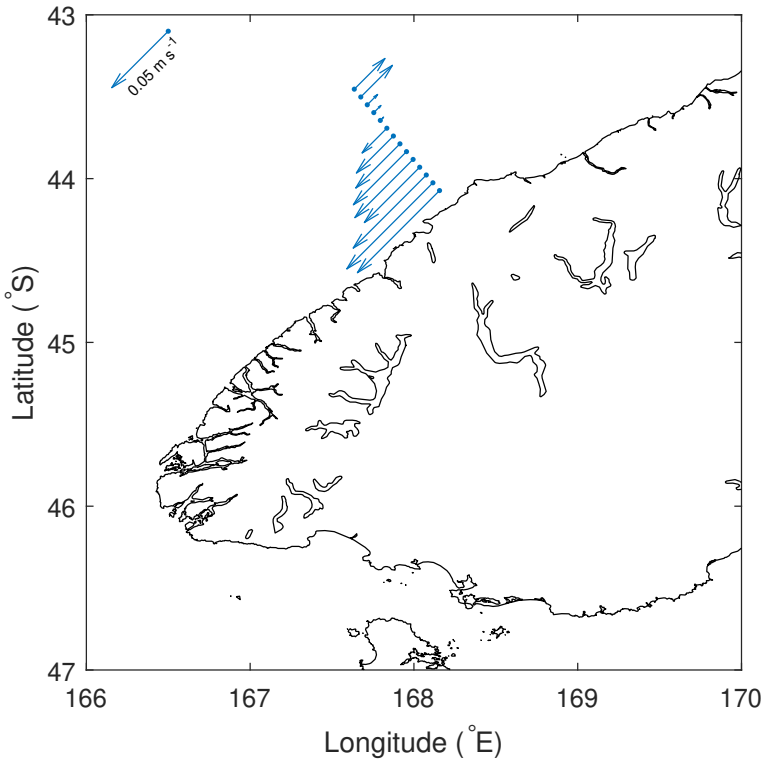

Figure A.3: Mean-state across-track surface geostrophic current for September 1992 – May 2017 offshore of the Fiordland coast for altimeter track 112 referenced to the 1993–2012 period. The maximum velocity is 0.08 $\mathrm{m\,s^{-1}}$ poleward. A 0.05 $\mathrm{m\,s^{-1}}$ reference arrow is included in the top left.

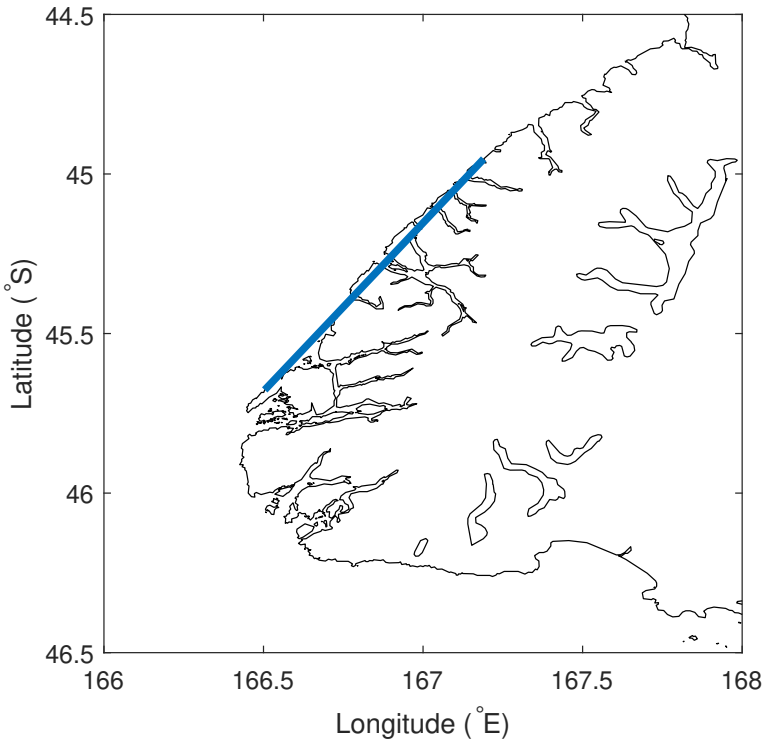

Figure A.4: Straight-line estimate of the Fiordland coastline (blue line) between 45.6767° S 166.5036° E and 44.9529° S 167.1900° E used for projecting the wind vectors onto to calculate the alongshore component of the wind stress.

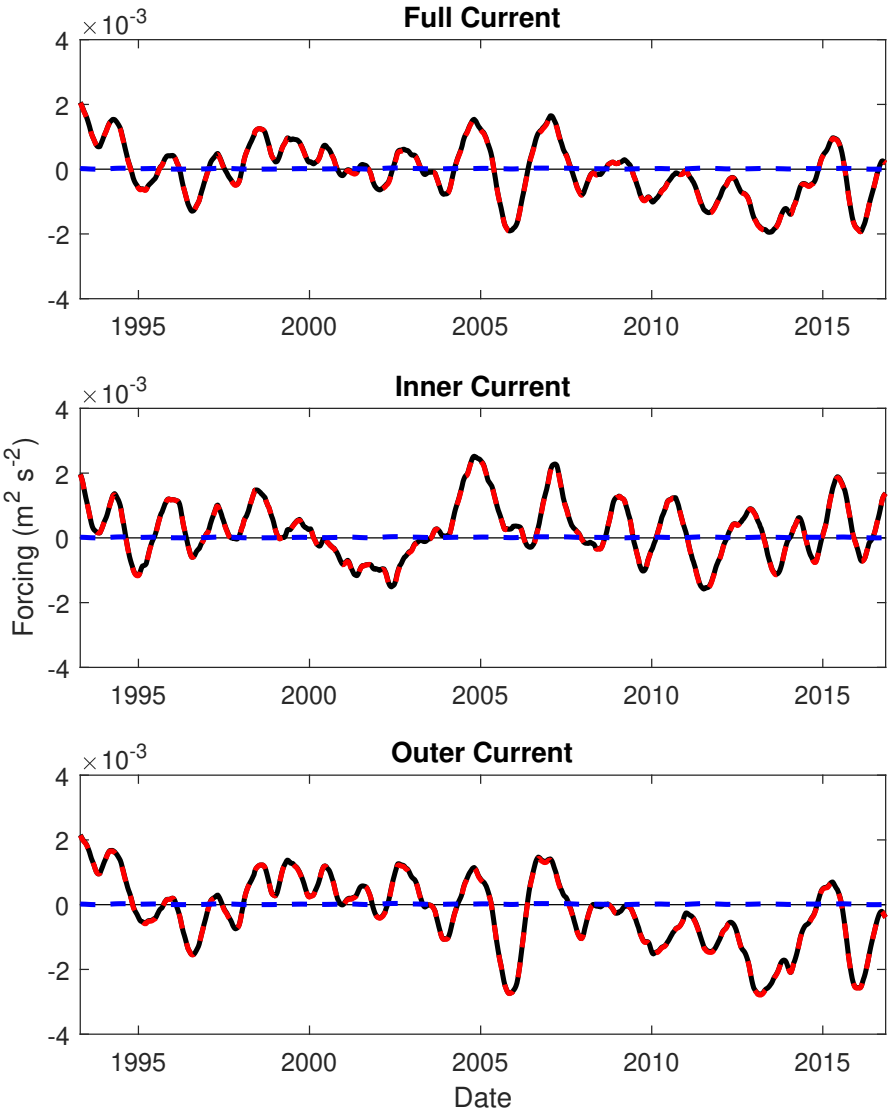

Figure A.5: Annually-smoothed alongshore pressure gradient anomaly (red dashed line), alongshore wind stress (blue dashed line), and combined (solid black line) forcing terms ($m^2\,s^{-2}$) depth-integrated to a reference level of 2000 m for the full (top), inner (middle), and outer (bottom) extents of the Fiordland Current over the altimeter record (April 1993 – November 2016). Negative forcings are poleward.

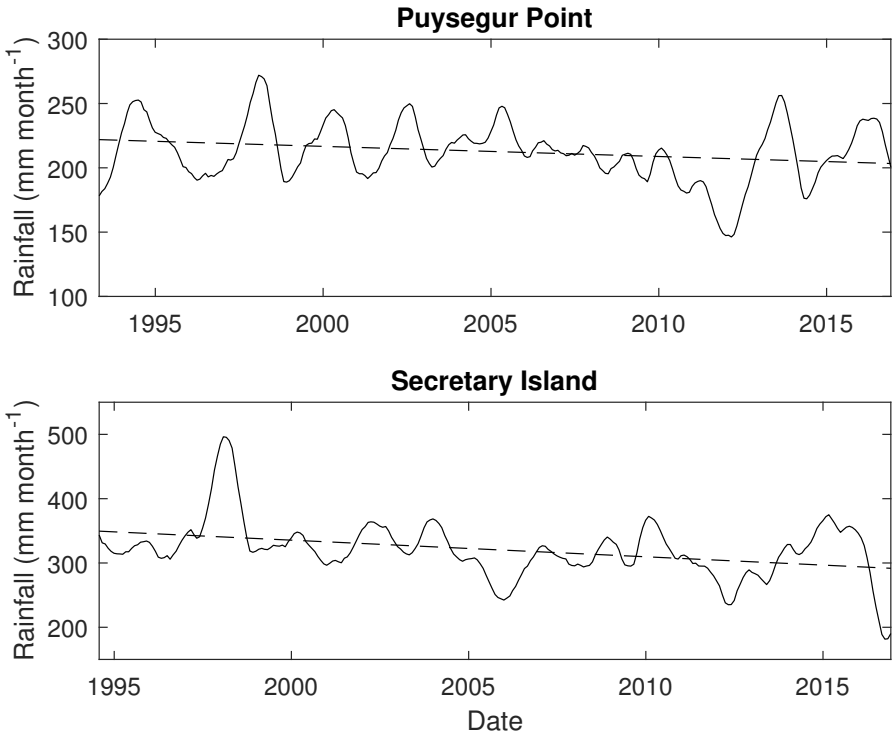

Figure A.6: Annually-smoothed rainfall (mm month^{-1}) for (top) Puysegur Point (46.156° S 166.613° E, April 1993 – November 2016) and (bottom) Secretary Island (45.221° S 166.886° E, July 1994 – November 2016). Dashed lines are the linear trend (Puysegur Point = -7.87 ± 8.78 mm month^{-1} decade^{-1}, Secretary Island = -25.85 ± 19.85 mm month^{-1} decade^{-1}). Note the different time-scales on the x-axis.

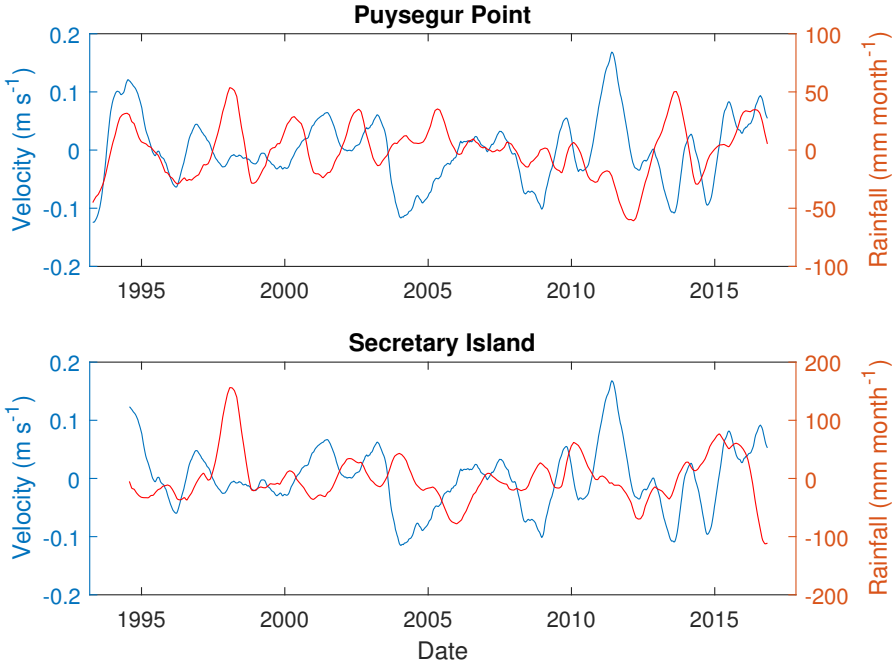

Figure A.7: Detrended annually-smoothed across-track surface geostrophic velocity anomaly (m s^{-1}) for the inner Fiordland Current and detrended annually-smoothed rainfall (mm month^{-1}) over the altimeter record for (top) Puysegur Point (46.156° S 166.613° E, April 1993 – November 2016) and (bottom) Secretary Island (45.221° S 166.886° E, July 1994 – November 2016). Negative velocities represent poleward anomalies. Correlation coefficients are r = −0.05, p = 0.716, EDOF = 55 for Puysegur Point, and r = −0.13, p = 0.388, EDOF = 46 for Secretary Island.